PROJECT TITLE

Design and Optimization of Plasmonic Refractive Index Sensors Using Concentric Resonators and Wire Gratings.

Masrur Ibne Ali (200021131)

Mustafid Bin Mostafa (200021141)

Imtiaz Tanweer Rahim (200021150)

Report on

EEE 4700_4800 (Project and Thesis)

Department of Electrical and Electronic Engineering

Islamic University of Technology (IUT)

Gazipur, Bangladesh

October 2025

DECLARATION

We hereby certify that the thesis titled “**Design and Optimization of Plasmonic Refractive Index Sensors Using Concentric Resonators and Wire Gratings.**" represents the outcome of research conducted under the supervision of Dr. Rakibul Hasan Sagor, Professor at the Islamic University of Technology. This work fulfills partial requirements for the degree of Bachelor of Science in Electrical and Electronic Engineering at IUT. We affirm that this thesis or any part of it has not been previously submitted for any other degree or diploma. Proper attribution has been given to all consulted sources and published works of others.

We affirm that this thesis or any part of it has not been previously submitted for any other degree or diploma. Proper attribution has been given to all consulted sources and published works of others.

Signature of the Candidates:

Masrur Ibne Ali

Student ID: 200021131

Mustafid Bin Mostafa

Student ID: 200021141

Imtiaz Tanweer Rahim

Student ID: 200021150

THESIS TITLE

Design and Optimization of Plasmonic Refractive Index Sensors Using Concentric Resonators and Wire Gratings.

Approved by:

Dr. Rakibul Hasan Sagor

Supervisor and Professor,

Department of Electrical and Electronic Engineering,

Islamic University of Technology (IUT),

Boardbazar, Gazipur-1704.

Date: ……

Acknowledgments

We would like to express our profound gratitude and sincere appreciation to all those who have supported and guided us throughout the journey of this research.

First and foremost, we offer our deepest gratitude to our supervisor, Dr. Rakibul Hasan Sagor, Professor, Department of Electrical and Electronic Engineering, for his invaluable guidance, unwavering support, and constant encouragement. His profound knowledge, insightful feedback, and patience were instrumental in shaping this thesis and navigating the challenges of our research. We are truly fortunate to have had the opportunity to learn under his mentorship.

We extend our sincere thanks to the Department of Electrical and Electronic Engineering at the Islamic University of Technology (IUT) for providing the necessary resources and an excellent academic environment that made this work possible.

Our heartfelt thanks go to our families for their unconditional love, endless support, and steadfast belief in our abilities. Their sacrifices and encouragement have been our greatest source of strength throughout our academic journey.

We are also grateful to our friends and colleagues for their camaraderie, stimulating discussions, and for creating a supportive and collaborative atmosphere. Finally, we acknowledge the developers of the COMSOL Multiphysics software, which was an essential tool for the simulations conducted in this work.

This accomplishment would not have been possible without the collective support of everyone mentioned above. Thank you.

Masrur Ibne Ali

Mustafid Bin Mostafa

Imtiaz Tanweer Rahim

October 2025

Abstract

Plasmonic refractive index (RI) sensors, while pivotal in biosensing and chemical detection, face limitations with conventional materials like gold and silver, including high optical losses and fabrication incompatibility. This thesis explores the design, optimization, and performance evaluation of advanced plasmonic sensing platforms to address these challenges. We propose and numerically analyze a novel metal-insulator-metal (MIM) waveguide-based sensor featuring a multi-layered composite resonator with an integrated nanorod array. The structure's performance is rigorously optimized, demonstrating a maximum sensitivity of 1800 nm/RIU and a Figure of Merit (FOM) of 34.0 for the optimal 10-nanorod configuration. Furthermore, we investigate Titanium Nitride (TiN) as an alternative plasmonic material, achieving a sensitivity of 1800 nm/RIU, thereby validating its potential as a durable and CMOS-compatible substitute. In parallel, we design and optimize plasmonic grating circuits based on triangular and circular geometries for surface plasmon resonance (SPR) sensing. The triangular grating sensor achieves a sensitivity of 600 nm/RIU and a high FOM of 80.28 RIU^{-1}, outperforming many existing grating-based sensors. Collectively, this work demonstrates significant advancements in plasmonic sensor design through innovative resonator geometries and the integration of alternative materials, paving the way for highly sensitive, robust, and practical sensing applications.

Keywords

1. Plasmonic Sensor
2. Refractive Index Sensing
3. Metal-Insulator-Metal (MIM) Waveguide
4. Titanium Nitride (TiN)
5. Grating Coupled Surface Plasmon Resonance (GCSPR)

List of Abbreviations

- CMOS: Complementary Metal-Oxide-Semiconductor
- FDTD: Finite-Difference Time-Domain
- FEM: Finite Element Method
- FOM: Figure of Merit
- FWHM: Full Width at Half Maximum
- GCSPR: Grating Coupled Surface Plasmon Resonance
- LSP: Localized Surface Plasmon
- LSPR: Localized Surface Plasmon Resonance
- MIM: Metal-Insulator-Metal
- NIR: Near-Infrared
- OBE: Outcome-Based Education
- PO: Program Outcome
- Q-factor: Quality Factor
- RI: Refractive Index
- RIU: Refractive Index Unit
- SP: Surface Plasmon
- SPP: Surface Plasmon Polariton
- SPR: Surface Plasmon Resonance
- TiN: Titanium Nitride
- TMN: Transition-Metal Nitride
- ZrN: Zirconium Nitride

Table of Contents

Introduction........ 1
1.1 Background on plasmonics........ 1
1.2 RI sensor, grating circuits and alternative material........ 3
1.3 Background and motivation........ 6
Overview of Workflow........ 8
2.1 Literature review of RI sensors........ 8
2.2 Proposed Design of RI Sensor........ 10
2.2.1 Proposed Structure........ 10
2.2.2 Optimization........ 12
2.2.3 Performance Analysis........ 13
2.3 Analysis with alternative plasmonic materials........ 17
2.3.1 Literature Review........ 17
2.3.2 Using TiN........ 18
2.3.3 Performance analysis using TiN........ 19
2.3.4 Result comparison with previous studies........ 22
2.4 Grating Circuits........ 23
2.4.1 Literature Review:........ 23
2.4.2 SPR Sensor Based on Triangular Grating........ 24
2.4.2.1 Design........ 24
2.4.2.2 Simulation Results and Analysis........ 25
2.4.3 SPR Sensor Based on Circular Grating........ 31
2.4.3.1 Design........ 31
2.4.3.2 Simulation results and analysis........ 32
2.4.4 Comparison Between Two Systems and Previous Works........ 37
Future Work........ 39
Conclusion........ 40
References........ 41
Demonstration of Outcome-Based Education (OBE)........ 45
5.1 Introduction........ 45
5.2 Course Outcomes (COs) Addressed........ 45
5.3 Aspects of Program Outcomes (POs) Addressed........ 46
5.4 Knowledge Profiles (K3 – K8) Addressed........ 47
5.5 Use of Complex Engineering Problems........ 49
5.6 Socio-Cultural, Environmental, And Ethical Impact........ 49
5.7 Attributes of Ranges of Complex Engineering Problem Solving (P1 – P7) Addressed........ 49
5.8 Attributes of Ranges of Complex Engineering Activities (A1 – A5) Addressed........ 51

List of Figures

Fig. 1.1 The evanescent electric field distribution of a surface plasmon polariton (SPP) at the interface between a metal and a dielectric.-- 2

Fig. 1.2 A conceptual figure of a typical MIM-based plasmonic RI sensor------------------------------3

Fig. 1.3 Comparison of conventional material vs alternative-- 6

Fig. 2.2.1 (a) Multilayered-composite Resonator consisting of both Square and Hexagonal Cavities (b) Sensor with all its dimensions labelled-- 10

Fig. 2.2.2 Wavelength vs Transmittance profile-- 11

Fig. 2.2.3 (a) Multilayered-composite Resonator consisting of both Square and Hexagonal Cavities with an array of 6 nanorods (b) with 10 nanorods (c) with 18 nanorods (d) dimensions as per Table 2.2.1 and r = 15 nm-- 12

Fig. 2.2.4 (a) Transmittance vs Wavelength (Parametric Sweep) profile of the composite Resonator without nanorods (b) with 6 nanorods (c) with 10 nanorods (d) with 18 nanorods--------------------12

Fig. 2.2.5: Resonance range and corresponding sensitivity profile for the structure with 10 nanorods representing (a) Mode-1 (b) Mode-2 (c) Mode-3 (d) Mode-4 and (e) Mode-5-------------------------16

Fig. 2.2.6 Surface Electric field at frequency (a) 444.94THz (b) 371.1 THz (c) 355.6 THz (d) 291.9 THz and (e) 207.3 THz-- 17

Fig. 2.3.1 Various properties of TiN [23]---18

Fig. 2.3.2 (a) Design of the composite sensor with TiN without nanorods (b) with 10 nanorods (c) with 14 nanorods (d) Transmittance vs Wavelength (Parametric Sweep) profile of the composite resonator without nanorods (e) with 10 nanorods (f) with 14 nanorods--------------------------------19

Fig. 2.3.3 Resonance range and corresponding Sensitivity profile for the structure with no nanorods representing (a) Mode-1 (b) Mode-2 and (c) Mode-3-- 21

Fig. 2.3.4 Surface Electric field at frequency (a) 381.46 THz (b) 304.42 THz (c) 211.9THz------- 21

Fig. 2.4.1 (a) 3D view of triangular grating circuit (b) Comsol model for triangular grating-------- 24

Fig. 2.4.2 Reflection spectra with different periods.-- 26

Fig. 2.4.3 Reflection spectra of different values of n for a grating period of (a) 520 nm. (b) 540 nm (c) 560 nm (d) 580 nm and (e) 600 nm--- 26

Fig. 2.4.4 Relationship between resonant wavelength and refractive index for grating period of (a) 520 nm (b) 540 nm (c) 560 nm (d) 580 nm and (e) 600 nm--- 27

Fig. 2.4.5 Electric field distribution for the periodicity value of (a) 520 nm (b) 540 nm (c) 560 nm (d) 580 nm and (e) 600 nm.-- 29

Fig. 2.4.6 (a) Variation of FOM vs Periodicity (b) Variation of Sensitivity vs Periodicity (c) Variation of FWHM with respect to Duty Cycle-- 30

Fig. 2.4.7 (a) 3D view of circular grating circuit (b) Comsol model for circular grating------------- 31

Fig. 2.4.8 Reflection spectra with different periods.-- 32

Fig. 2.4.9 Reflection spectra of different values of n for a grating period of (a) 520 nm. (b) 540 nm (c) 560 nm (d) 580 nm and (e) 600 nm--- 33

Fig. 2.4.10 Relationship between resonant wavelength and refractive index for grating period of (a) 520 nm (b) 540 nm (c) 560 nm (d) 580 nm and (e) 600 nm--- 34

Fig. 2.4.11 Electric field distribution for the periodicity value of (a) 520 nm (b) 540 nm (c) 560 nm (d) 580 nm and (e) 600 nm.-- 36

Fig. 2.4.12 (a) Variation of FOM vs Periodicity (b) Variation of Sensitivity vs Periodicity (c) Variation of FWHM with respect to Duty Cycle-- 37

List of Tables

Table 2.2.1: Geometric properties of the resonator at the initial stage-----------------------------------10

Table 2.2.2: maximum Sensitivity and corresponding FOM obtained for the various configurations of the sensors.--- 14

Table 2.3.1: Maximum Sensitivity and corresponding FOM obtained for the various configurations of the sensors.--- 19

Table 2.3.2: MIM-based Plasmonic Sensors-- 22

Table 2.3.3: Plasmonic Sensors based on Alternative Materials--- 22

Table 2.4.1: Parameters and description of the proposed sensor--- 25

Table 2.4.2: Variation of sensitivity with periodicity values--- 27

Table 2.4.3: Variation of FOM vs Periodicity---29

Table 2.4.4: Performance metrics comparison for SPR Sensor based on Triangular Grating-------- 30

Table 2.4.5: Parameters for Circular Grating-- 32

Table 2.4.6: Variation of Sensitivity with Periodicity values-- 34

Table 2.4.7: Variation of FOM vs Periodicity---36

Table 2.4.8: Performance metrics comparison for SPR Sensor based on Circular Grating.---------- 37

Table 2.4.9: Comparison between circular and triangular grating-------------------------------------- 37

Table 2.4.10: Comparison between Previous Literature Works--- 38

Chapter 1
Introduction

1.1 Background on plasmonics

Plasmons are collective oscillations of free electrons in a metal, meaning many electrons move together in response to external energy like light. These oscillations give metals special optical properties. The dielectric constant εm is described by:

$$\epsilon_m = 1 - \frac{\omega_p^2}{\omega^2} \tag{1.1}$$

The bulk plasma frequency, denoted as ωp, defines a critical threshold for light interaction. At frequencies lower than ωp, the material's electrons oscillate in phase with the incoming light, effectively reflecting it. Conversely, for light with a frequency exceeding ωp, the electrons cannot oscillate rapidly enough to cancel out the electromagnetic field, resulting in transmission.

At the metal-dielectric interface, surface plasmons (SPs) can couple with photons to form surface plasmon polaritons (SPPs), which are surface-bound electromagnetic waves. It is important to note that not all light can naturally excite SPP waves. To generate SPPs, the momentum of the incoming light must match that of the SPP wave. However, light in free space usually doesn't have enough momentum to match the SPPs. This mismatch can be fixed by using special techniques like prisms, gratings, optical fibers, or waveguides; these tools help increase the light's momentum so it can couple properly with the SPP.

$$k_{SPP} = k\sqrt{\frac{\epsilon_d \epsilon_m}{\epsilon_d + \epsilon_m}} \tag{1.2}$$

The formula that equation (1.2) describes how SPPs behave is called the dispersion relation. Here, d and m are the permittivities (a measure of how a material responds to electric fields) of the dielectric and metal, respectively. This equation shows that the SPP has more momentum and a shorter wavelength than regular light in free space for the same frequency. SPPs are excited most efficiently when the permittivities of the metal and dielectric satisfy:

$$\epsilon_d + \epsilon_m = 0 \tag{1.3}$$

At this point, the frequency of the SPP becomes:

$$\omega_{SPP} = \frac{\omega_p}{\sqrt{1+\epsilon_d}} \tag{1.4}$$

It can be seen that the SPP frequency is lower than the bulk plasma frequency p. Once the SPP is excited, it doesn't go deep into the materials. Instead, it creates an evanescent field that stays close to the surface and fades away quickly, deeper in the dielectric, and even more quickly in the metal.

In dielectric, the electric field decays exponentially with distance, this decay length is called δd. In the metal, the decay is even faster, this decay length is δm. So, the SPP's field is mostly "squeezed" near the surface and quickly fades away in both directions. The reason δd > δm is that the metal's electrons respond more strongly to the field, blocking deeper penetration.

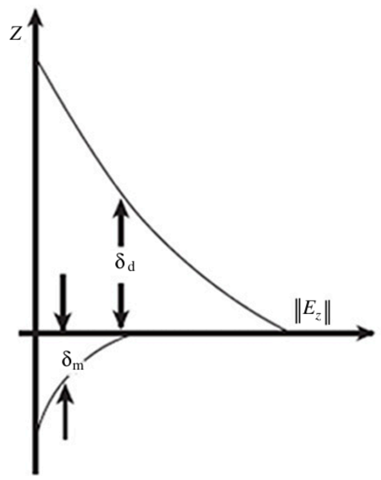

Fig. 1.1 The evanescent electric field distribution of a surface plasmon polariton (SPP) at the interface between a metal and a dielectric.

In contrast, localized surface plasmons (LSPs) form on tiny metal particles like nanoparticles. These don't travel along a surface like SPPs, they just vibrate in place when hit by light. These vibrations, called localized surface plasmon resonances (LSPR), don't require special setups to match momentum; they can be directly excited by shining light on the nanoparticle. LSPRs create very strong electric fields in tiny regions, making them perfect for sensing applications.[8]

1.2 RI sensor, grating circuits and alternative material

The field of plasmonic sensing has expanded dramatically since Nylander and Liedberg's pioneering work on thin metal film SPR for refractive index sensing three decades ago [7,8]. This technology has seen significant commercial development, broadening its user base considerably. As a mature technology today, conventional SPR sensing provides the definitive benchmark against which all emerging nanoplasmonic sensors must be measured.A plasmonic refractive index sensor based on a Metal-Insulator-Metal (MIM) waveguide is a compact optical device that utilizes surface plasmon polaritons (SPPs) to detect changes in the refractive index of a surrounding medium. The MIM structure consists of a dielectric layer (insulator) sandwiched between two metal layers (typically silver or gold), allowing tight confinement of SPPs, which enhances sensitivity and miniaturization.

A MIM-based plasmonic refractive index sensor operates by guiding surface plasmon polaritons through a narrow dielectric layer between two metals. When the refractive index of the surrounding environment changes (due to analyte binding or material variation), the effective index and resonance conditions of the SPP modes shift. This shift can be detected as a change in transmission spectrum, resonance wavelength, or phase, making the structure highly sensitive for biosensing and chemical sensing applications.

MIM waveguides are preferred due to:

- Strong field confinement.
- Compatibility with integrated photonic circuits.
- High sensitivity to refractive index changes.

Basic Structure and Operation:

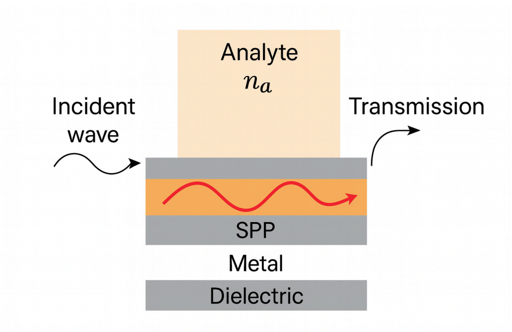

Fig. 1.2 A conceptual figure of a typical MIM-based plasmonic RI sensor

SPR Sensors Based on Grating Circuit:

Surface plasmon resonance (SPR) has become a foundational technology in optical sensing, prized within biological and chemical research for its ability to perform real-time, label-free detection [14-16]. The operating principle hinges on the high sensitivity of SPR sensors to alterations in the refractive index of the medium adjacent to the metal surface [17,18]. Such index changes manifest spectrally as distinct absorption peaks at characteristic wavelengths [19,20].

Advancements in nanofabrication have intensified interest in using nanostructured metals to excite SPR [21,22]. Specifically, periodic nanostructures facilitate this by supplying a supplementary wave vector. This extra component bridges the momentum mismatch between the wave vector of light in free space and that of the surface plasmon polariton [23,24]. For instance, one study created crossed surface relief gratings, achieving a notable sensitivity of 647.8 nm/RIU and a figure of merit (FOM) of 14 [25]. Despite their high performance, such intricate nanostructures involve complex fabrication that limits scalability. Conversely, metal gratings with simpler geometries, like circular or triangular profiles, are far more manufacturable while maintaining efficient SPR excitation [26,27]. This practicality underscores the need for optimizing grating-coupled SPR (GCSPR) sensors under real-world experimental constraints.

While prior research has compared sinusoidal and rectangular gratings by adjusting slit width to gauge sensitivity [28], the present work expands the optimization to include critical parameters like grating period and duty cycle. The experimental setup involves measuring reflection spectra under normal polychromatic light incidence, with the operating wavelength selected to align with the optimal detection range of silicon-based detectors.

A common pitfall in sensor evaluation is the independent consideration of metrics like sensitivity, FOM, and absorption peak depth, which can obscure the overall optimal configuration. Therefore, this study focuses on sensitivity and FOM as the primary, integrated indicators of sensor performance.

Regarding the optical phenomenon, when diffracted light couples into a waveguide, a corresponding dip is observed in the zeroth-order transmitted intensity. Conversely, a sharp intensity peak appears in the reflection spectrum. This counterintuitive result is explained by the principle of reversibility: the same mechanism that allows light to couple into the waveguide also enables it to couple out.

Grating Modes:

● Natural resonant modes in periodic arrays of subwavelength scatterers.

● Lead to sharp resonances in scattering spectra, near RA wavelengths.

● Are distinct from RAs and LSPs in origin and behavior.

LSP vs GM Resonances:

● LSPs are localized, shape-dependent, and have lower Q-factors.

● GMs are delocalized, periodicity-induced, and possess higher Q-factors.

● GMs produce stronger, sharper features useful for sensing.

Field Modeling:

●Accurate modeling of GMs requires advanced methods like analytical regularization.

● Floquet theory and boundary conditions are central to capturing these resonances.

Alternative Materials:

Noble metals such as gold and silver are traditionally employed in plasmonic and optical metamaterial structures owing to their high direct-current (DC) conductivity and relatively low ohmic losses. However, at optical frequencies, these materials experience additional losses caused by interband transitions, which significantly affect their optical performance. Interband loss occurs when a valence electron absorbs a photon and transitions either to the Fermi level or from near the Fermi level to a higher, unoccupied conduction band. This phenomenon is responsible for the characteristic coloration of metals like copper and gold.

Fig. 1.3 illustrates the imaginary component of gold's permittivity within the optical spectrum, as reported by Johnson and Christy. This imaginary part represents the material's optical loss, which can be categorized into interband and intraband (Drude) losses. In gold, intra-band losses dominate in the near-infrared (NIR) region but decrease at shorter wavelengths.

To address these limitations and enhance sensor performance, recent advancements in photonic materials have shifted focus toward transition-metal nitrides (TMNs), which exhibit metallic behavior and exceptional stability across visible and NIR regimes. Among them, titanium nitride (TiN), zirconium nitride (ZrN), and hafnium nitride (HfN), members of the group IV-B nitrides, stand out due to their high carrier concentrations and favorable plasmonic properties.

The primary objective of this research is to evaluate the performance of plasmonic refractive index sensors when traditional noble metals are replaced with such alternative materials. By analyzing their optical and sensing characteristics, this work aims to contribute to the development of next-generation plasmonic sensors and promote the broader adoption of TMNs in advanced plasmonic applications.[6]

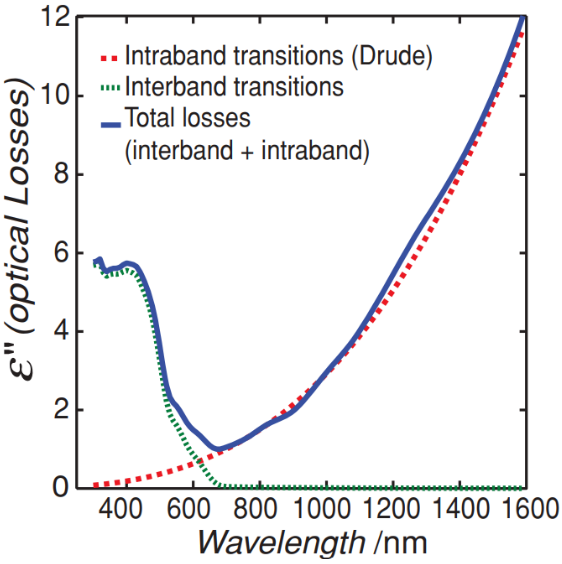

Fig. 1.3 Comparison of conventional material vs alternative

1.3 Background and motivation

Plasmonic refractive index sensors have become essential tools in diverse fields such as biosensing, chemical analysis, and environmental monitoring. These sensors operate based on the interaction of light with metallic nanostructures, traditionally gold and silver, to generate surface plasmon resonances (SPRs) that are highly responsive to variations in the surrounding refractive index [1]. In recent years, considerable research has focused on metal–insulator–metal (MIM)–based refractive index sensors due to their strong confinement of electromagnetic fields and excellent sensing performance. Such sensors have found practical use in numerous applications, including medical diagnostics [2].

Despite their extensive use, conventional plasmonic materials like gold and silver present several challenges, including significant optical losses, chemical instability (particularly in the case of silver), and a limited operational wavelength range [3]. Moreover, these noble metals are generally incompatible with standard silicon-based fabrication technologies, creating barriers to large-scale integration [3]. As the need for highly sensitive, robust, and versatile plasmonic devices continues to increase, these material constraints hinder further progress.

Recent advancements in materials science have drawn attention to alternative plasmonic materials such as graphene, titanium nitride (TiN), aluminum, and other transition metal nitrides, which offer improved optical, chemical, and thermal properties compared to traditional noble metals [3]. These materials not only provide broader spectral responses and lower losses but also exhibit greater stability, making them suitable candidates for next-generation sensing platforms. In addition, silicon-based plasmonic technologies have demonstrated the potential to miniaturize photonic components to deep subwavelength scales while enhancing optical emission, detection, and signal control [4]. Pellegrini et al. reported that although germanium-based sensing platforms may not always surpass the performance of gold-based systems, they can still achieve comparable enhancement factors, exceeding three orders of magnitude under suitable conditions [5]. Similarly, Rakib et al. introduced a CMOS-compatible comb-shaped plasmonic sensor based on a ZrN–Insulator–ZrN configuration that achieved remarkable sensitivity and figure of merit (FOM) values [6].

The present study is motivated by the need to address the inherent limitations of conventional plasmonic materials through the exploration of these emerging alternatives. The goal is to improve both the sensitivity and durability of plasmonic refractive index sensors, paving the way for their broader use in advanced applications such as medical diagnostics, environmental monitoring, and next-generation integrated photonic systems.

Chapter-2
Overview of Workflow

2.1 Literature review of RI sensors

Review of "A MIM Waveguide Structure of a High-Performance Refractive Index and Temperature Sensor Based on Fano Resonance" [24]

This study introduces a dual-parameter plasmonic sensor that detects both refractive index and temperature. The design features a metal-insulator-metal (MIM) waveguide coupled with two symmetrical rectangular baffles and a concentric double-ring resonator (CCDRR). Operating on the principle of Fano resonance, a result of destructive interference between broad and narrow resonant modes, the sensor achieves high sensitivity. Finite element method (FEM) simulations demonstrate a refractive index sensitivity of 2260 nm/RIU and a figure of merit (FOM) of 56.5, outperforming many existing sensors. The structure also functions as a temperature sensor when filled with ethanol, yielding a sensitivity of 1.48 nm/°C.

Strengths:

1. **Innovative Design:** The integration of a CCDRR with rectangular baffles in an MIM waveguide is a novel approach that effectively exploits Fano resonance for sensing applications. The design offers new detection positions and high sensitivity.
2. **Comprehensive Analysis:** The paper thoroughly investigates the effects of various geometric parameters (e.g., radii of the rings, baffle dimensions, coupling gap) on the sensor's performance, providing valuable insights for optimization.
3. **High Performance:** The achieved sensitivity (2260 nm/RIU) and FOM (56.5) are superior to many referenced designs, making the sensor competitive for practical applications.
4. **Dual Functionality:** The sensor's ability to measure both refractive index and temperature expands its potential applications, such as in biosensing and environmental monitoring.
5. **Clear Methodology:** The use of FEM and detailed simulations lends credibility to the results, and the paper is well-structured with clear explanations.

Weaknesses:

Experimental Validation: The study relies entirely on simulations.

Design of a Refractive Index Plasmonic Sensor Based on a Ring Resonator Coupled to a MIM Waveguide Containing Tapered Defects [2]

1. Objective: The paper presents a novel nanoscale refractive index sensor using a metal-insulator-metal (MIM) plasmonic waveguide coupled with a ring resonator featuring tapered defects. The goal is to enhance sensitivity and figure of merit (FOM) for biosensing applications.

2. Design and Methodology:

- The sensor consists of a silicon MIM waveguide (width = 100 nm) and a ring resonator with circular tapered defects.
- The finite-difference time-domain (FDTD) method is used for numerical simulations. Key parameters include ring radius, defect sizes, and coupling distance between the waveguide and resonator.

3. Performance Metrics:

- Sensitivity: Achieves a maximum of 1295 nm/RIU (refractive index unit).
- FOM: Reaches 159.6 RIU^{-1}, indicating high resolution.
- Detection Range: Operates for refractive indices from 1.00 to 1.65.

4. Key Findings:

- Introducing tapered defects in both the waveguide and ring resonator significantly improves FOM and sensitivity.
- The optimal structure (with defects in both components) achieves the highest performance metric (P.M.= 97), combining FOM and transmittance variation.
- The sensor exhibits a linear response to refractive index changes, suitable for precise measurements.

5. Comparison: Outperforms recent plasmonic sensors in FOM and sensitivity (e.g., FWHM=8.11 nm). Compact size and high resolution make it ideal for integrated optical circuits and biosensing.

Strengths:

- High FOM and sensitivity.
- Comprehensive parametric analysis and clear comparison with existing sensors.

Limitations:

- Reliance on simulations without experimental validation.
- Fabrication complexity due to nanoscale defects.

2.2 Proposed Design of RI Sensor

2.2.1 Proposed Structure

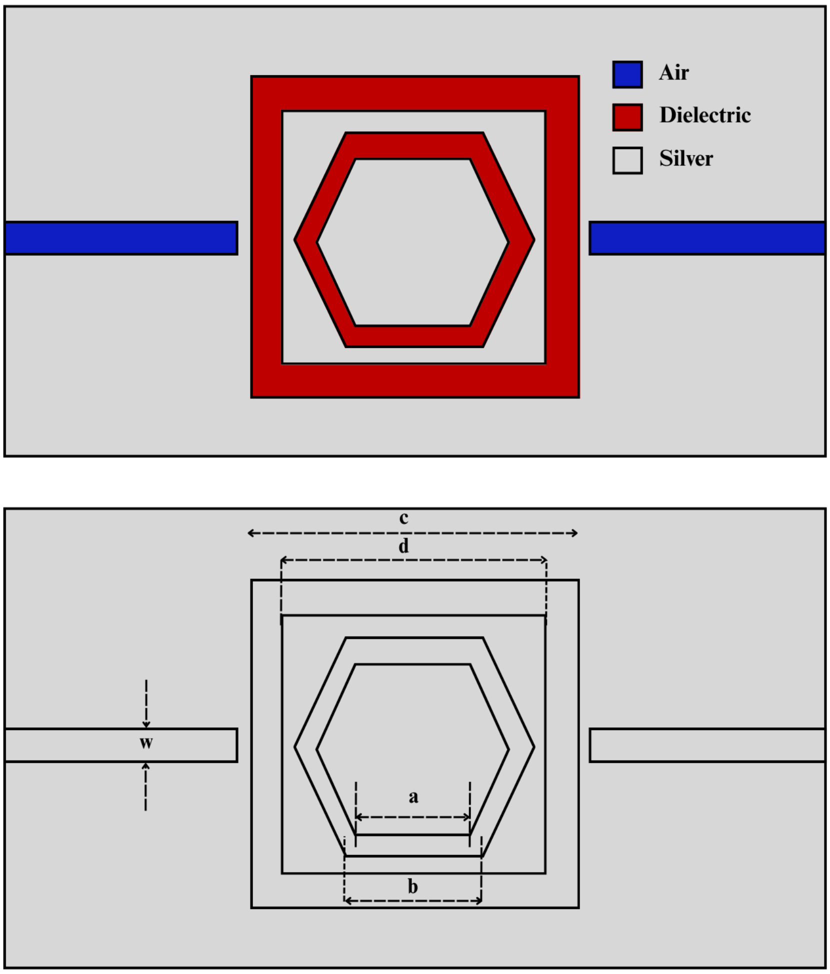

Fig. 2.2.1 (a) Multilayered-composite Resonator consisting of both Square and Hexagonal Cavities (b) Sensor with all its dimensions labelled

Table 2.2.1: Geometric properties of the resonator at the initial stage

Name of the parameter	Symbol	Value (nm)
Width of the inner Hexagon	a	200
Width of the outer Hexagon	b	150
Width of the outer Rectangle	c	550
Width of the inner Rectangle	d	450
Width of the Waveguide	w	50

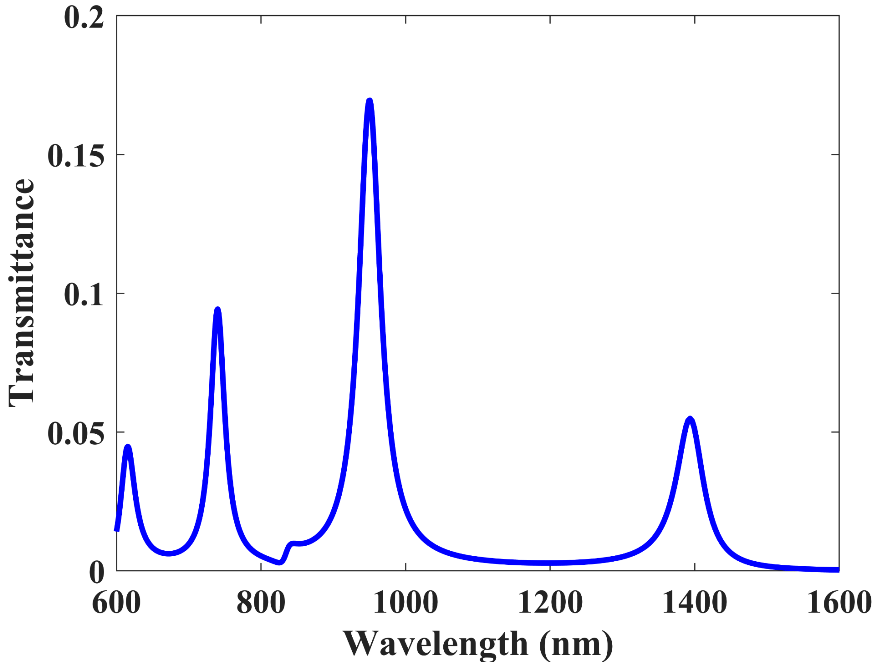

Fig. 2.2.2 Wavelength vs Transmittance profile

Motivation behind the structural design: The two papers [17,18] demonstrate that plasmonic refractive index sensors using concentric resonator structures, either double-square or double-ring, within metal–insulator–metal (MIM) waveguides can achieve high sensitivity, narrow resonance linewidths, and strong light–analyte interaction. Both designs show that optimizing resonator geometry enhances sensing performance, making them promising candidates for biosensing and on-chip optical integration.

Our Design: In our case, we design a central nested hexagonal cavity resonator, made up of two concentric hexagons. These hexagons are enclosed within a square cavity, forming a multi-layered composite resonator. On both sides, narrow waveguides are connected, allowing light to couple into and out of the cavity. This structure is designed to support localized surface plasmon resonances (LSPRs) and guided wave resonances, with the nested hexagons enhancing field confinement and mode interference. The hexagonal symmetry may also promote multiple resonance modes due to its multi-angle geometry [19].

2.2.2 Optimization

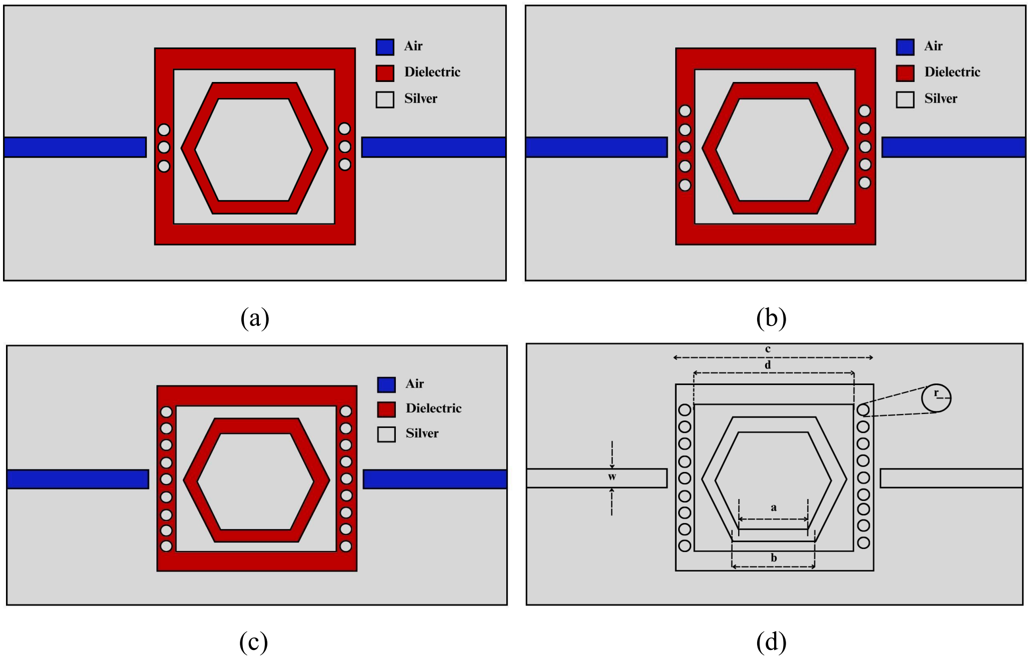

Fig. 2.2.3 (a) Multilayered-composite Resonator consisting of both Square and Hexagonal Cavities with an array of 6 nanorods (b) with 10 nanorods (c) with 18 nanorods (d) dimensions as per Table 2.2.1 and r = 15 nm

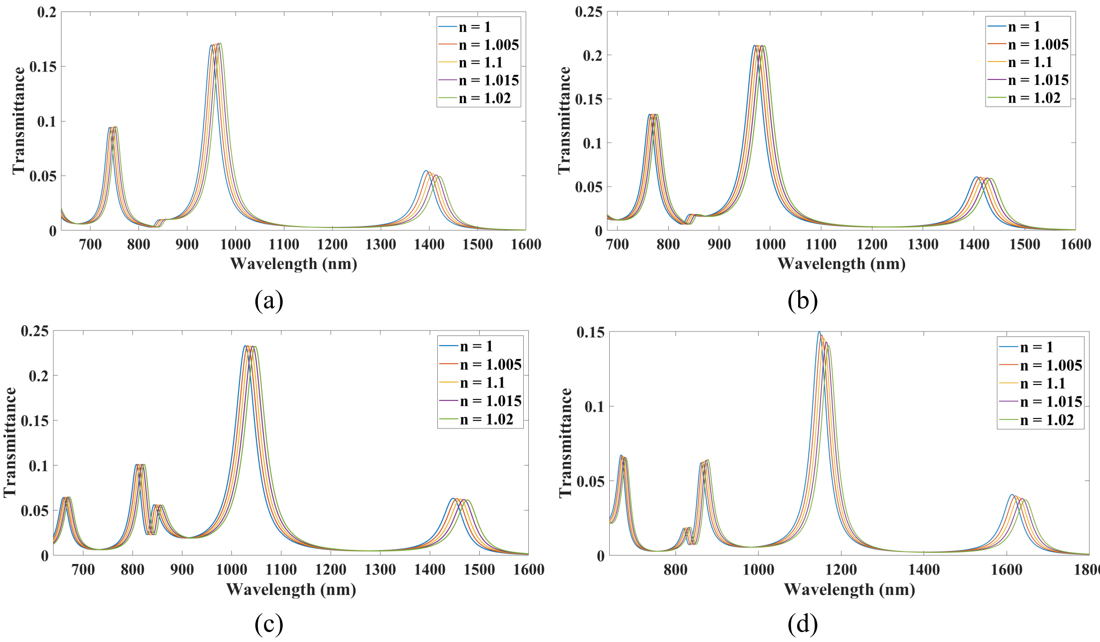

Fig. 2.2.4 (a) Transmittance vs Wavelength (Parametric Sweep) profile of the composite Resonator without nanorods (b) with 6 nanorods (c) with 10 nanorods (d) with 18 nanorods

As seen in Fig. 2.2.4, the transmittance spectra evolve significantly as nanorods are added to the composite resonator. In the absence of nanorods (a), the resonances appear sharp, strong, and highly transmissive, showing minimal loss. With six nanorods (b), the peaks begin to broaden and their intensity decreases due to additional plasmonic absorption and scattering, while a slight red shift of the resonance positions becomes noticeable. This red shift continues and becomes more pronounced as the number of nanorods increases to ten (c) and eighteen (d), reflecting the stronger plasmon photon coupling and the effective increase in the optical path length within the resonator. At the same time, the overall transmittance falls steadily, with the sharp peaks giving way to weaker, broader responses. Importantly, the shift toward longer wavelengths is often linked to better sensitivity, since small refractive index changes can induce larger measurable spectral shifts at these wavelengths. However, this improvement in sensitivity comes at the cost of a lower figure of merit (FOM), because the broadened peaks reduce spectral resolution. In short, adding nanorods enhances light–matter interaction and sensitivity, but the tradeoff is reduced transmission efficiency and a lower FOM due to broader, damped resonance peaks.

2.2.3 Performance Analysis

Sensitivity (S) is one of the most important design and performance metrics for refractive index (RI) sensors. It describes how accurately the sensor can detect even small variations in the refractive index and is mathematically defined by the following equation [2],

$$S = \frac{d\lambda}{dn} \tag{2.1}$$

where $d\lambda$ = shift in resonance wavelength, dn = change in refractive index

The Figure of Merit (FOM) is an important parameter used to assess a sensor's overall performance by combining both its sensitivity and precision. It indicates how effectively the sensor can resolve small refractive index variations in a material. Mathematically, the **FOM** is defined as the ratio of the sensor's sensitivity (S) to the Full Width at Half Maximum (**FWHM**) of its resonance peak, as given by the following equation [2],

$$FOM = \frac{S}{FWHM} \tag{2.2}$$

The Quality Factor (Q-factor) of a refractive index (RI) sensor represents the ratio between its resonant wavelength and the Full Width at Half Maximum (FWHM). It reflects how sharp and well-defined the resonant peak is. The Q-factor is mathematically expressed by the following equation [2],

$$Q = \frac{\lambda_{resonance}}{FWHM} \tag{2.3}$$

Table 2.2.2: maximum Sensitivity and corresponding FOM obtained for the various configurations of the sensors.

Structural Configuration	**Sensitivity (S) (nm/RIU)**	**Figure of Merit (FOM)**
No nanorods	1400	32.6
6 nanorods	1600	33.3
10 nanorods	**1800**	**34.0**
18 nanorods	1600	29.9

The comparison of different structural configurations shows that introducing nanorods improves the sensitivity of the sensor compared to the case without nanorods. Without nanorods, the sensitivity is **1400 nm/RIU** with a FOM of **32.6**. When 6 nanorods are added, the sensitivity increases to **1600 nm/RIU**, and the FOM also improves slightly to **33.3**. With 10 nanorods, the sensitivity remains the same at **1800 nm/RIU**, but the FOM reaches its highest value of **34.0**, indicating sharper and more efficient resonance performance. However, when the number of nanorods is increased further to 18, although the sensitivity still stays at **1600 nm/RIU**, the FOM decreases to **29.9**, suggesting significant peak broadening and a reduction in resolution. Considering both sensitivity and figure of merit, the configuration with 10 nanorods offers the best balance. It provides high sensitivity along with the highest FOM, meaning it can detect small refractive index changes effectively while maintaining good spectral sharpness. Therefore, the **10-nanorod configuration** is the most suitable candidate for use as a biosensor.

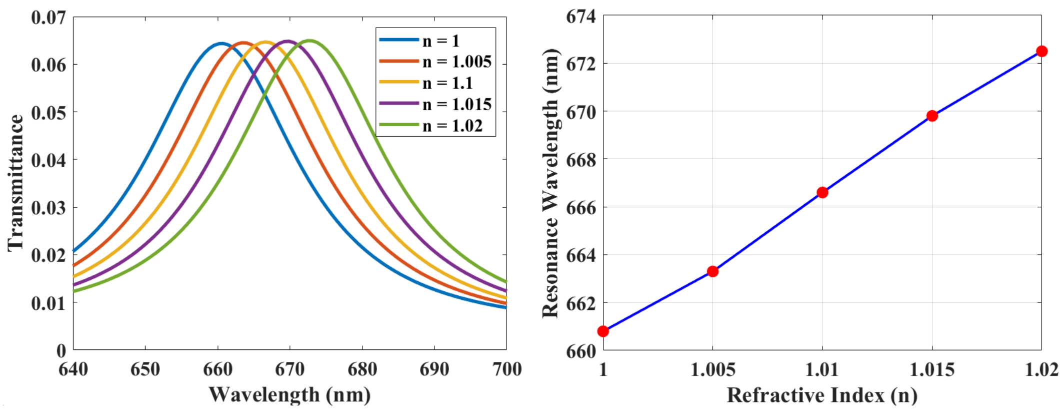

(a)

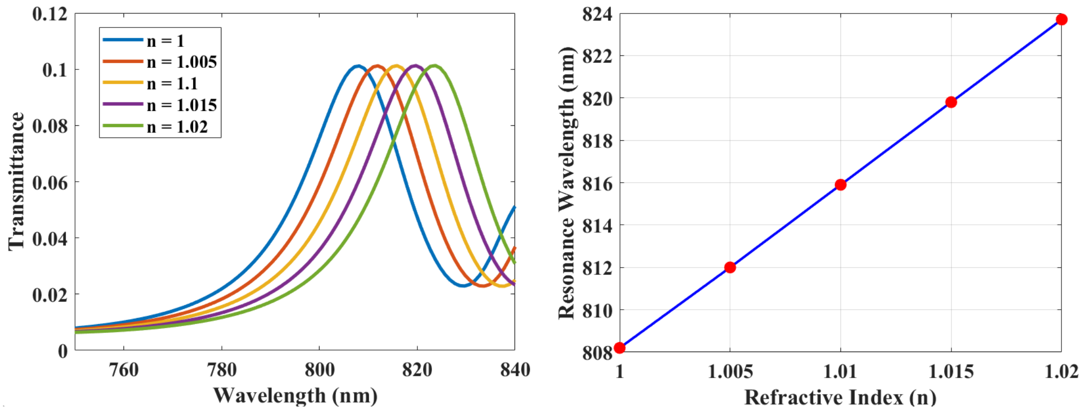

Transmittance
Wavelength (nm)
n = 1
n = 1.005
n = 1.1
n = 1.015
n = 1.02
0.12
0.1
0.08
0.06
0.04
0.02
0
760
780
800
820
840
Resonance Wavelength (nm)
Refractive Index (n)
824
822
820
818
816
814
812
810
808
1
1.005
1.01
1.015
1.02

(b)

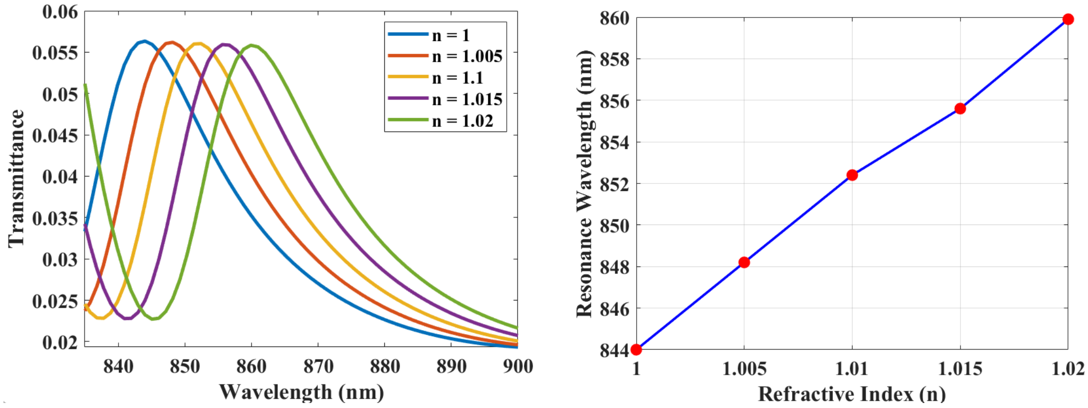

Transmittance
Wavelength (nm)
n = 1
n = 1.005
n = 1.1
n = 1.015
n = 1.02
0.06
0.055
0.05
0.045
0.04
0.035
0.03
0.025
0.02
840
850
860
870
880
890
900
Resonance Wavelength (nm)
Refractive Index (n)
860
858
856
854
852
850
848
846
844
1
1.005
1.01
1.015
1.02

(c)

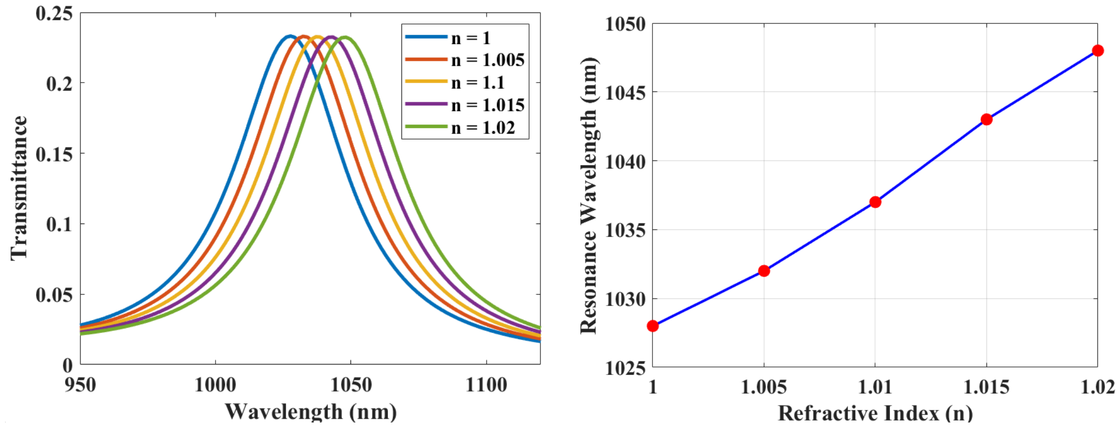

Transmittance
Wavelength (nm)
n = 1
n = 1.005
n = 1.1
n = 1.015
n = 1.02
0.25
0.2
0.15
0.1
0.05
0
950
1000
1050
1100
Resonance Wavelength (nm)
Refractive Index (n)
1050
1045
1040
1035
1030
1025
1
1.005
1.01
1.015
1.02

(d)

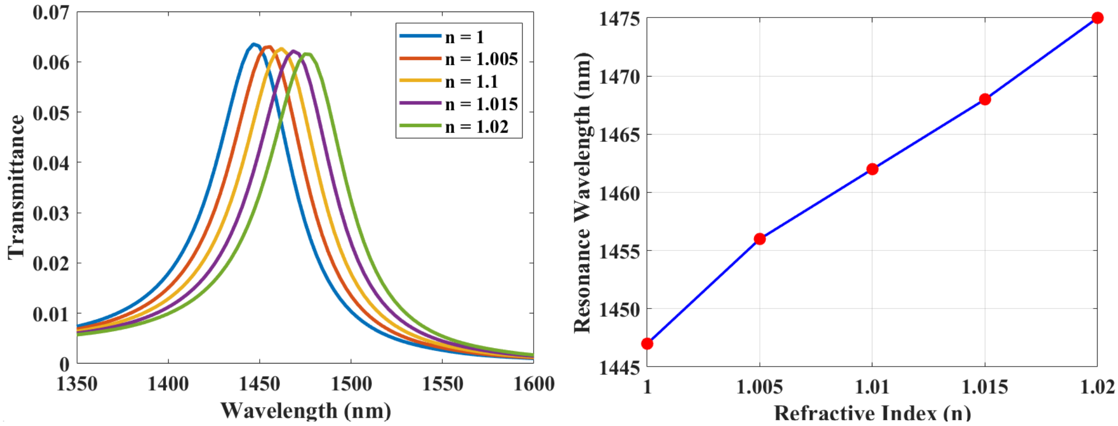

(e)

Fig. 2.2.5: Resonance range and corresponding sensitivity profile for the structure with 10 nanorods representing (a) Mode-1 (b) Mode-2 (c) Mode-3 (d) Mode-4 and (e) Mode-5

Fig. 2.2.5 presents the resonance range and sensitivity profile for the structure with 10 nanorods across five modes. In all cases, an increase in refractive index from **1.00** to **1.02** causes a consistent redshift in the resonance wavelength, confirming a strong index-dependent response. **Mode 1 (≈ 660–673 nm)** shows a small but steady shift, while the shift magnitude increases in **Mode 2 (≈ 808–824 nm)** and **Mode 3 (≈ 844–860 nm)**. Higher modes, **Mode 4 (≈ 1025–1050 nm)** and **Mode 5 (≈ 1445–1475 nm)**, exhibit the largest wavelength changes, indicating higher sensitivity at longer wavelengths. Overall, the resonance peaks move linearly or near-linearly with refractive index for all modes, showing stable and predictable sensing behavior with progressively increasing sensitivity from Mode 1 to Mode 5.

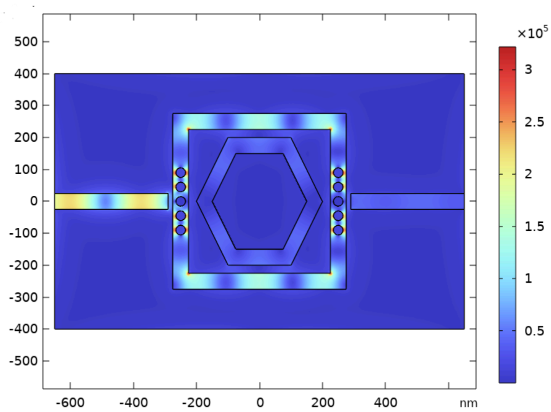

(a)

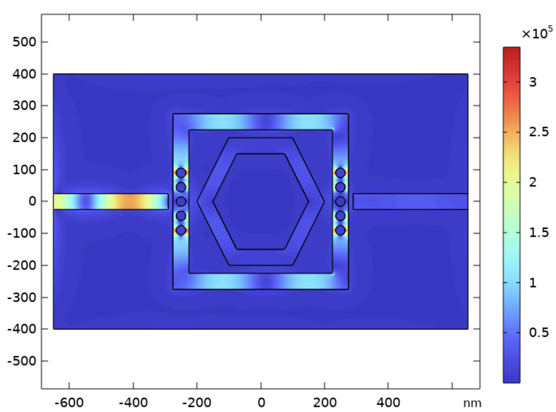

(b)

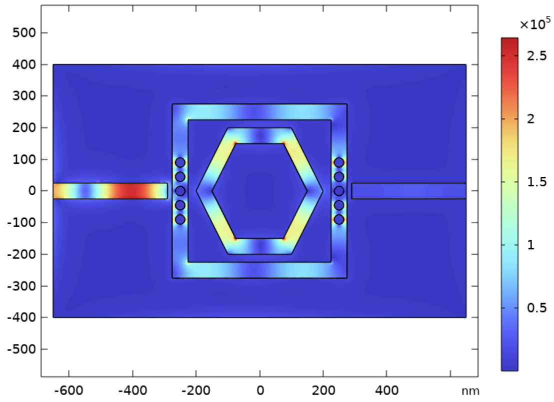

(c)

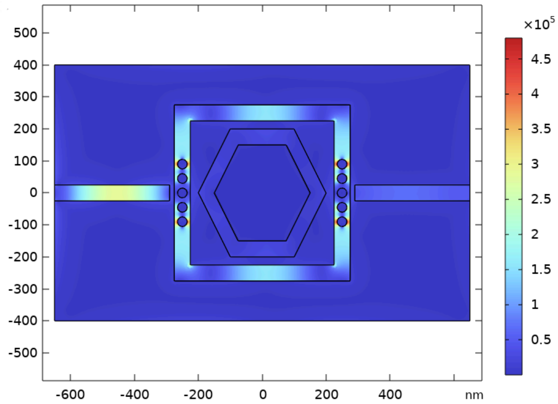

(d)

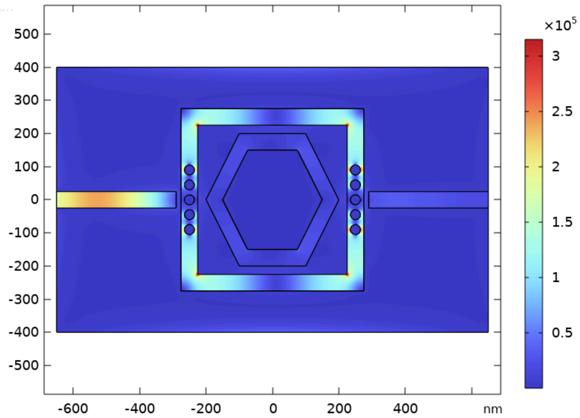

(e)

Fig. 2.2.6 Surface Electric field at frequency (a) 444.94THz (b) 371.1 THz (c) 355.6 THz (d) 291.9 THz and (e) 207.3 THz

Fig 2.2.6 displays the surface electric field (Hz) distributions at frequencies **444.94 THz**, **371.1 THz**, **355.6 THz**, **291.9 THz**, and **207.3 THz**. Each pattern shows a distinct field distribution around the resonator and the nanorod region, varying with frequency. At higher frequencies (a, b), the field is more concentrated and exhibits stronger contrast near the coupling region, while at lower frequencies (c-e), the field spreads more uniformly with weaker intensity differences. Overall, the variation across frequencies highlights distinct modal patterns for each resonance condition, with the distribution gradually expanding as the frequency decreases.

2.3 Analysis with alternative plasmonic materials

2.3.1 Literature Review

Titanium Nitride (TiN) is becoming a strong alternative to traditional plasmonic materials like gold and silver, especially in biomedical implants and electrochemical sensing. One of the biggest reasons is its excellent biocompatibility, it works well with the human body and doesn't cause harmful immune reactions, unlike silver, which can sometimes be toxic in biological environments. TiN is also much more durable; while gold and silver are soft and wear down over time, TiN is highly resistant to wear and corrosion, making it ideal for implants that need to last inside the body for years. In sensing applications, TiN offers great electrical conductivity, which helps detect signals more accurately. It also stays stable even in harsh or corrosive environments, where gold or silver might degrade. For this reason, we try to explore the use of this material instead of traditional plasmonic materials for sensing purposes.[23]

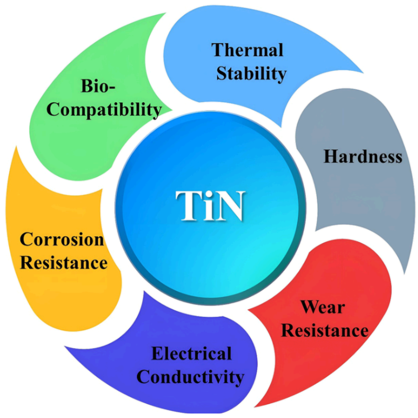

Fig. 2.3.1 Various properties of TiN [23]

2.3.2 Using TiN

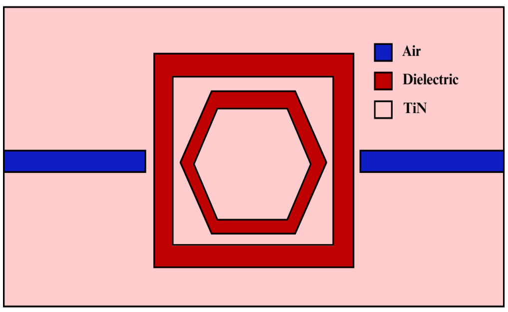

(a)

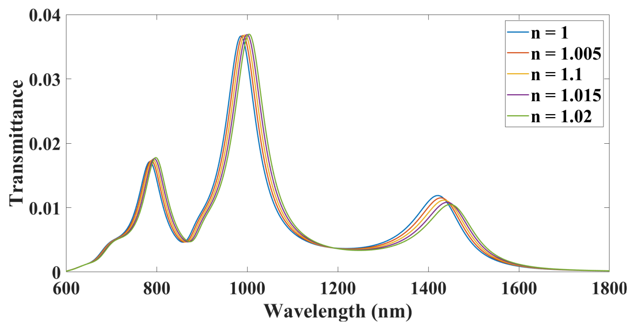

(d)

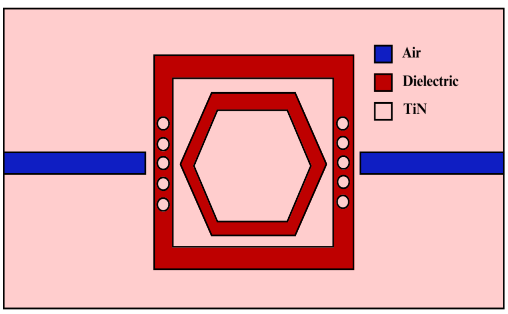

(b)

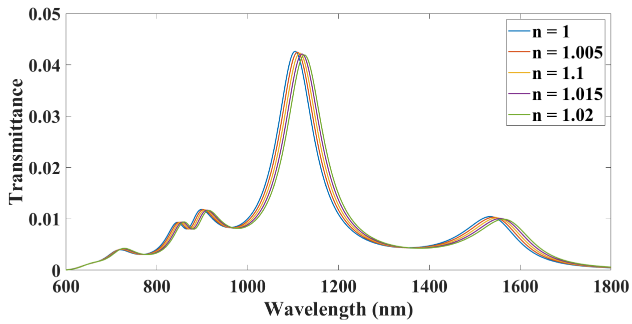

(e)

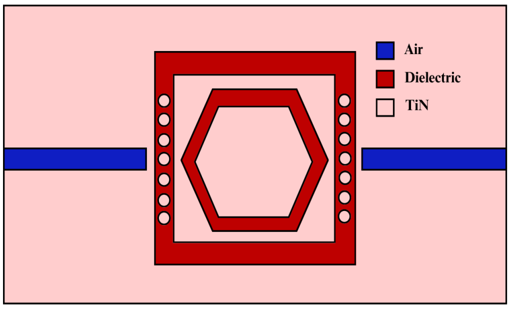

(c)

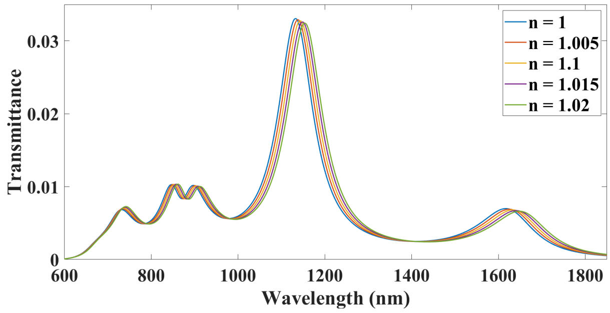

(f)

Fig. 2.3.2 (a) Design of the composite sensor with TiN without nanorods (b) with 10 nanorods (c) with 14 nanorods (d) Transmittance vs Wavelength (Parametric Sweep) profile of the composite resonator without nanorods (e) with 10 nanorods (f) with 14 nanorods

In Fig. 2.3.2, the transmittance spectra show clear differences across the three configurations. Without nanorods (d), the resonant peaks are sharp but the spectral shifts with refractive index are relatively small. With 10 nanorods (e), the peaks undergo a stronger redshift as the refractive index increases, and the resonance features remain comparatively well defined. When the number of nanorods is increased to 14 (f), the redshift becomes more pronounced, but the peaks broaden and their intensity decreases, indicating higher optical losses. Thus, increasing nanorod density enhances spectral shifts but also leads to broader, less intense resonances.

2.3.3 Performance analysis using TiN

Table 2.3.1: Maximum Sensitivity and corresponding FOM obtained for the various configurations of the sensors.

Structural Configuration	Sensitivity (S) (nm/RIU)	Figure of Merit (FOM)
No nanorods	**1800**	**16.1**
10 nanorods	1400	12.1
14 nanorods	1600	8.8

In our previous study involving silver-based nanostructures, introducing nanorods led to a clear increase in sensitivity because of stronger plasmonic coupling and enhanced light–matter interaction. However, in this case the results deviate from that trend. The configuration without nanorods already provides the highest sensitivity **(1800 nm/RIU)** and the best figure of merit (FOM) (**16.1**). When nanorods are introduced, the sensitivity does not consistently improve, dropping to **1400 nm/RIU** with 10 nanorods and only slightly rising to **1600 nm/RIU** with 14 nanorods, while the FOM decreases sharply in both cases. This shows that, unlike silver-based nanorod systems where plasmonic enhancement dominates, here the addition of nanorods introduces more optical losses and resonance broadening, reducing overall sensing performance.

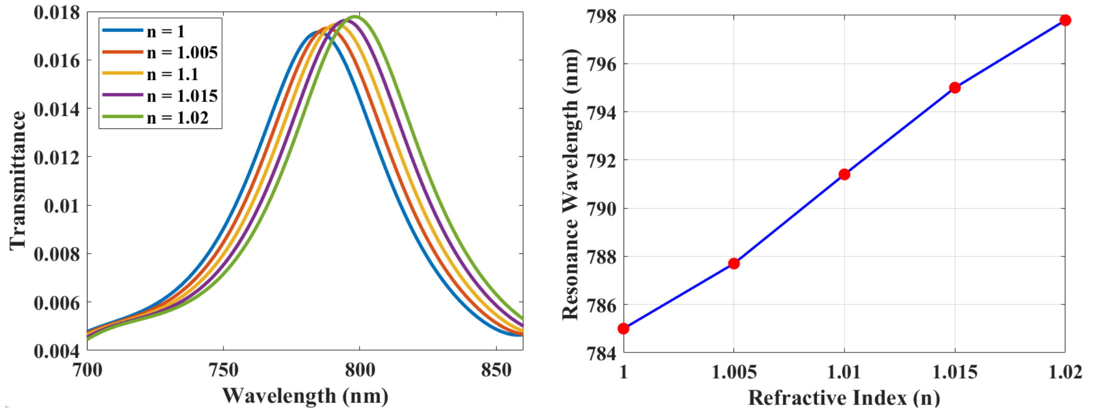

(a)

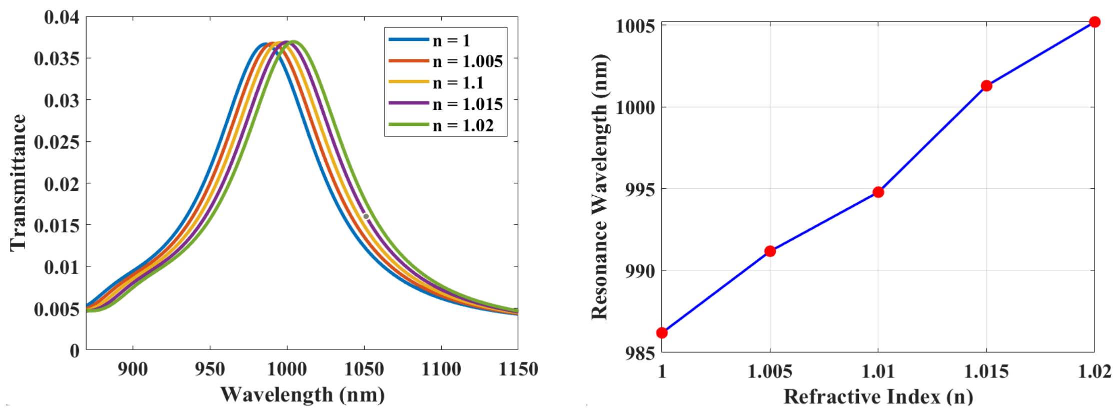

(b)

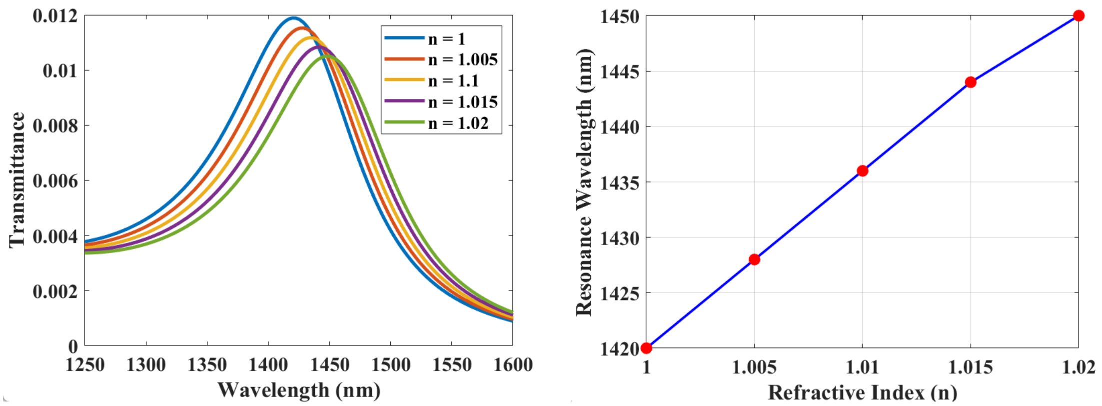

(c)

Fig. 2.3.3 Resonance range and corresponding Sensitivity profile for the structure with no nanorods representing (a) Mode-1 (b) Mode-2 and (c) Mode-3

Fig 2.3.3 shows that for all three modes, the resonance wavelength redshifts progressively as the refractive index increases from 1.00 to 1.02, indicating a clear refractive-index sensitivity. In **Mode 1 (≈ 785–798 nm)**, the shift is modest; in **Mode 2 (≈ 986–1005 nm)**, the shift becomes more pronounced; and in **Mode 3 (≈ 1417–1446 nm)**, the wavelength change is the largest, demonstrating higher sensitivity at longer wavelengths. The nearly linear relation between resonance wavelength and refractive index across all modes confirms stable and predictable sensing behavior, with Mode 3 offering the strongest response among them.

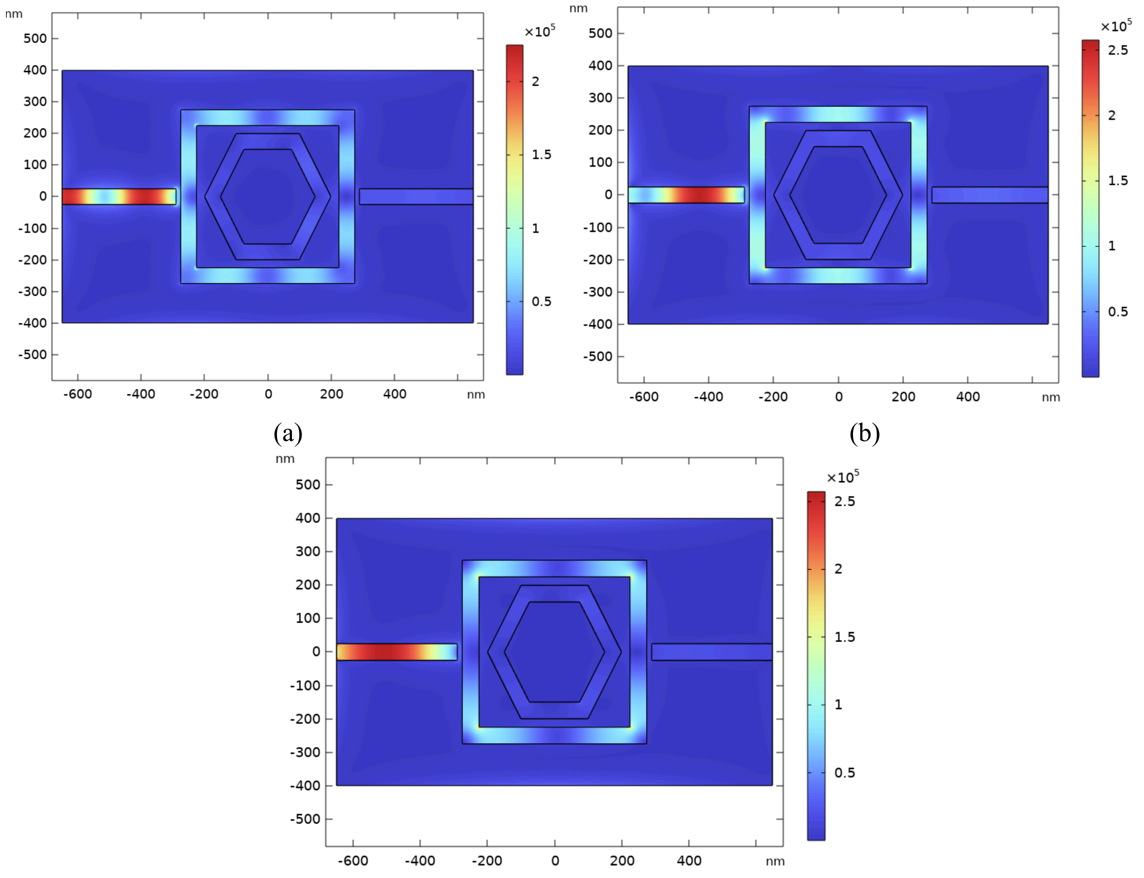

Fig. 2.3.4 Surface Electric field at frequency (a) 381.46 THz (b) 304.42 THz (c) 211.9THz

Fig. 2.3.4 shows the surface electric field (Hz) distributions at three resonance frequencies, **381.46 THz**, **304.42 THz**, and **211.9 THz**. The field patterns vary distinctly with frequency, showing different levels of intensity and spread around the structure. At higher frequencies(a, b), the field is more concentrated near the resonator region, while at the lower frequency(c), it appears more uniformly distributed over a larger area. These variations clearly illustrate how the field profile changes with frequency across the three modes.

2.3.4 Result comparison with previous studies

Table 2.3.2: MIM-based Plasmonic Sensors

Reference	**Year**	**Max Sensitivity** (nm/RIU)	**FOM** (RIU^{-1})
MohammadReza Rakhshani [38]	2020	1055	19.5
Rabiul Al Mahmud et al. [39]	2020	2325	46
Mahdiye Rahmatiyar et al. [40]	2020	1295	159.6
Nikolay L. Kazanskiy et al. [37]	2021	700	21.9
Rizwanur Rahad et al. [41]	2024	1960	15.2
This work	-	1800	34

Table 2.3.3: Plasmonic Sensors based on Alternative Materials

Reference	**Year**	**Max Sensitivity** (nm/RIU)	**FOM** (RIU^{-1})
Infiter Tathfif et al. [35]	2021	1074.88	32.4
A.K.M Rakib et al. [6]	2023	1445.26	140.96
Rummanur Rahad et al. [36]	2024	913	36.52
This work	-	1800	16.1

2.4 Grating Circuits

2.4.1 Literature Review:

Review of "Optimization of plasmonic sensors based on sinusoidal and rectangular gratings" [28]

Grating-coupled surface plasmon resonance (GC-SPR) sensors are attractive for compact, label-free refractive-index sensing because periodic metal nanostructures supply the additional momentum needed to excite surface plasmons without a prism. The paper by Long et al. addresses optimization of three common grating geometries (sinusoidal, rectangular continuous metal, and rectangular discontinuous metal) to maximize a composite performance metric (FOM*), taking into account sensitivity, resonance linewidth (FWHM), and absorption peak depth, the latter added because shallow peaks are more susceptible to spectral noise. They used a new parameter called FOM* that is defined as -

$$FOM^{*} = FOM \times (absorption\, peak\, depth) \tag{2.4}$$

They used this parameter to jointly consider sensitivity, linewidth, and depth arguing this better reflects experimental detectability than S or FOM alone.

Strengths:

- **Clear, practical optimization:** concrete design numbers useful for experimental fabrication (period/depth/thickness/duty cycle).
- **Realistic constraints:** period chosen to fit silicon detector response (practical engineering tradeoff).
- **Comprehensive parametric maps** (reflection maps, field distributions) that help interpret spectral features and mode origins.
- **Use of a combined metric (FOM*)** acknowledges that depth matters for experimental detection limit (noise-limited)

Limitations:

- **Material scope limited to silver:** while silver gives narrower peaks, gold is more chemically stable and commonly used in biosensing; the paper does not compare alternative plasmonic materials (Al, Au, Cu, doped semiconductors, refractory plasmonics) or composite/bimetallic structures that may improve stability or extend spectral range.

● **Only normal incidence / wavelength interrogation:** angular interrogation and combined angular–wavelength modalities can yield different tradeoffs; the work focuses on normal incidence which is appropriate for many compact sensors but limits generality.

● **Noise model not explicit:** FOM* includes peak depth as a proxy for robustness to noise, but a quantitative noise model (detector noise, spectrometer resolution, sample scattering) and resulting limit of detection (LOD) estimation are not provided.

●**Fabrication tolerances/robustness:** the paper reports optimal nominal geometries but does not analyze sensitivity to fabrication errors (depth/duty cycle variations, edge roughness) or aging/oxidation of Ag. These are crucial for experimental realization.

● **Biochemical functionalization effects:** the influence of common sensing layers (e.g., self-assembled monolayers, dielectric overlayers for selectivity) on the resonance and FOM* is not addressed.

2.4.2 SPR Sensor Based on Triangular Grating

2.4.2.1 Design

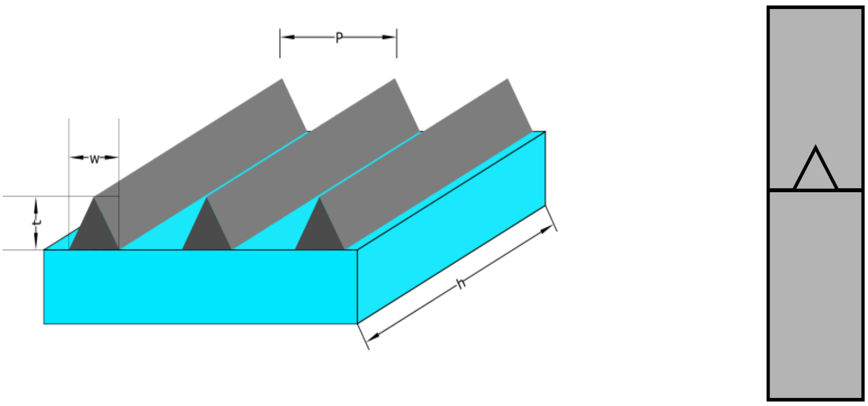

(a) (b)

Fig. 2.4.1 (a) 3D view of triangular grating circuit (b) Comsol model for triangular grating

Periodic Boundary Condition is applied on both sides of the grating circuit to indicate that the structure is periodically repeated throughout. Gratings are placed periodically on the top of the glass substrate and above that we place a sensing medium. The sensing media can be air or any solution whose change in refractive index will be sensed by the proposed system. The overall system works based on the principle of reversibility. The reflected light intensity peaks at the angle corresponding to light coupling into the waveguide and depends on the effective index of the waveguide mode such that the refractive index is reflected in the spectra by generating an absorption peak at a specific wavelength. The Floquet boundary condition is applied while solving the Maxwell's equation in the system.

Table 2.4.1: Parameters and description of the proposed sensor

Name	Expression	Value	Description
n_air	1	1	Refractive index of air
n_substrate	1.45	1.45	Refractive index of glass substrate
lambda	500[nm]	$0.15\mu m$	Wavelength of incident ray
tm	120[nm]	$0.25\mu m$	Height of grating
ts	1[um]	$3\mu m$	Height of substrate
h_clad	1000[nm]	$3\mu m$	Height of clad layer
a	550[nm]	$0.55\mu m$	Slit width
w	p×duty	$0.168\mu m$	Grating size
width	w + 2×d	$0.56\mu m$	Width of the substrate
p	560 [nm]	$0.56\mu m$	Periodicity
n	1	1	Refractive index of the sensing medium
duty	0.3	0.3	Duty cycle
d	$\frac{p-w}{2}$	$0.196\mu m$	Gap between grating and boundary

2.4.2.2 Simulation Results and Analysis

Based on the value of periodicity the transmittance peaks shift continuously to the right affecting the overall performance, sensitivity and FOM values.

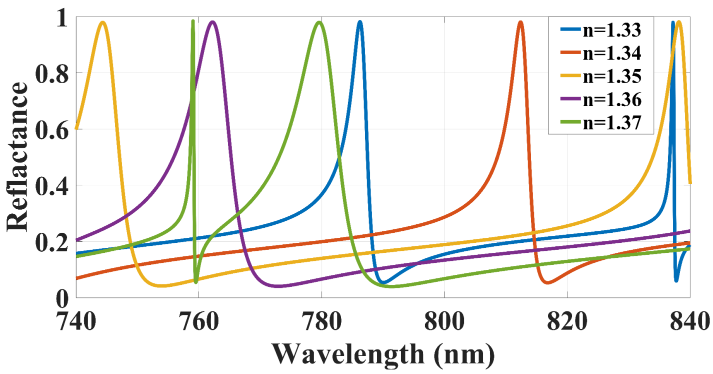

Fig. 2.4.2 Reflection spectra with different periods.

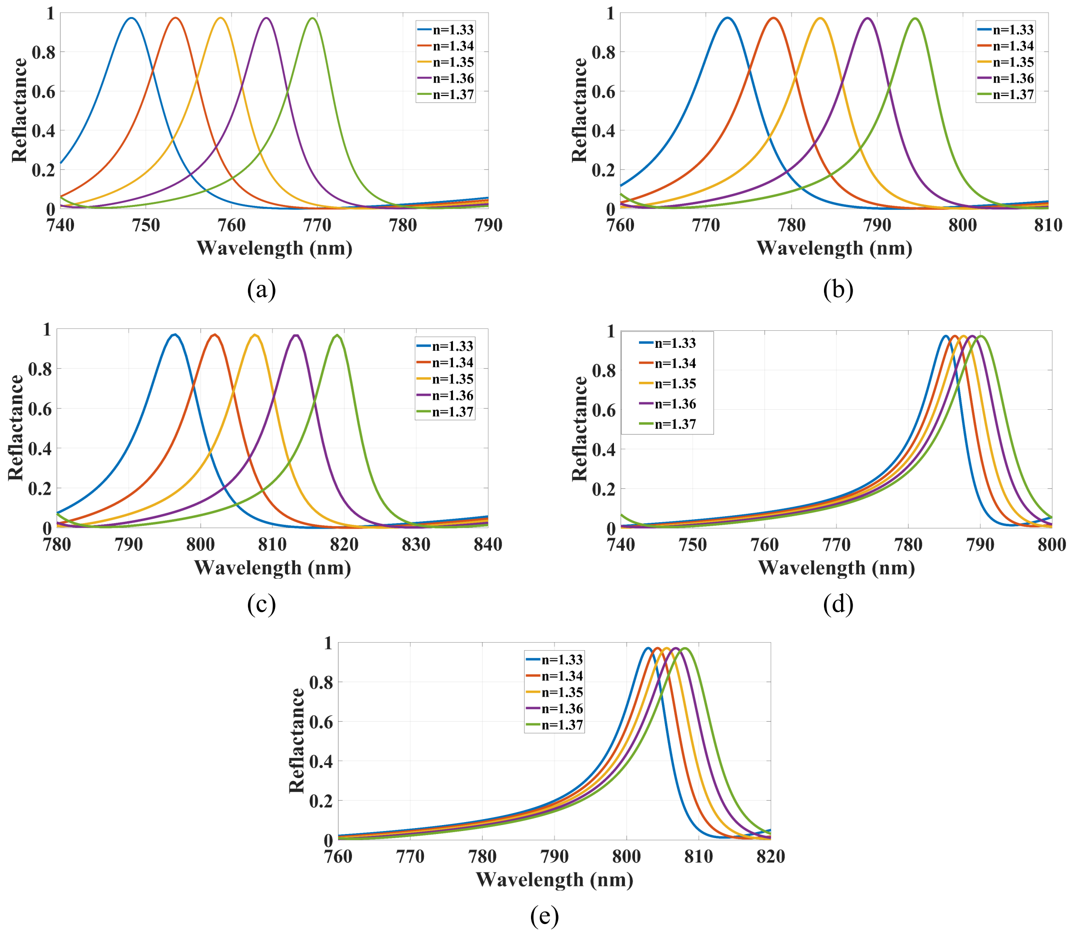

Fig. 2.4.3 Reflection spectra of different values of n for a grating period of (a) 520 nm. (b) 540 nm (c) 560 nm (d) 580 nm and (e) 600 nm

From **Fig. 2.4.3(c)**, we can observe the reflectance profile for the system for a grating period of **560 nm** and found the sensitivity value to be **600 nm/RIU**. As we changed the periodicity value from **520 nm** to **600 nm,** the resonant wavelength shifts as portrayed in Fig. 2.4.2.

As we shift the value of periodicity from 520 nm to 600 nm the resonant wavelength range changes from 740 nm to 780 nm for Fig. 2.4.3(a), 760 - 810 nm for Fig. 2.4.3(b), 780-840 nm for Fig. 2.4.3(c), 740-810 nm for Fig. 2.4.3(d) and 760-830 nm for Fig. 2.4.3(e).

Table 2.4.2: Variation of sensitivity with periodicity values

Periodicity value (nm)	Sensitivity (nm/RIU)
520	540
540	570
560	600
580	120
600	130

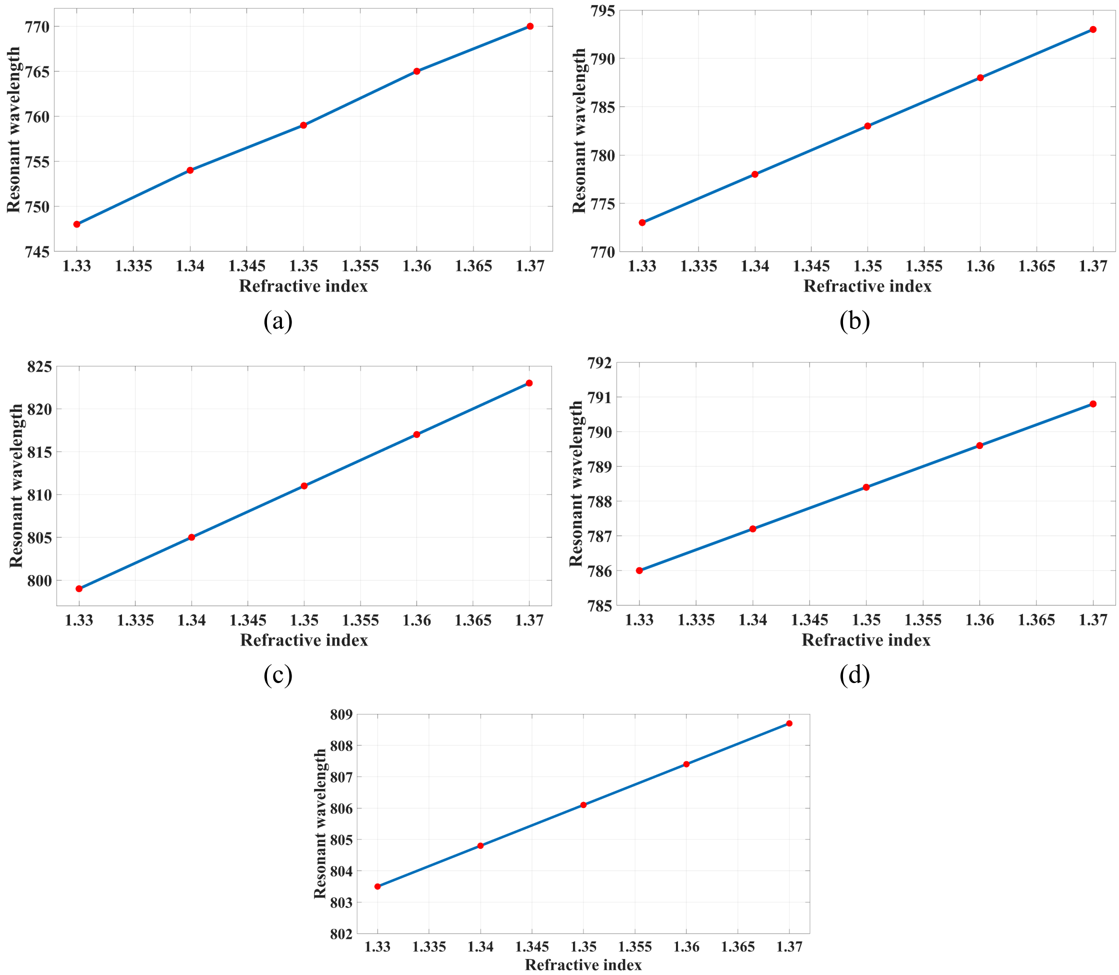

(e)

Fig. 2.4.4 Relationship between resonant wavelength and refractive index for grating period of (a) 520 nm (b) 540 nm (c) 560 nm (d) 580 nm and (e) 600 nm

As we change the value of the periodicity electric field distribution changes inside the grating circuit.

For p = **520 nm** in Fig. 2.4.5(a) most of the field energy leaks into the analyte region, maximizing sensitivity. This confirms the system is operating in the desired SPR mode, making it well-suited for refractive index sensing. The field maps depict a standing wave pattern characterized by angled, periodic fringes (alternating red/yellow for high magnitude and blue for low magnitude) in the regions above and below the boundary that contains the small triangular grating element. This pattern is the result of the interference between the incident wave and the waves reflected and diffracted by the grating structure.

Fig. 2.4.5(c) shows a stable, ordinary wave interference pattern, confirming that the grating system's electromagnetic response is insensitive to this minor variation in the refractive index. That is why for a periodicity value of **560 nm,** we got the highest value of sensitivity. On the other hand, increasing periodicity beyond 560 nm results in a significant decrease of sensitivity and FOM values.

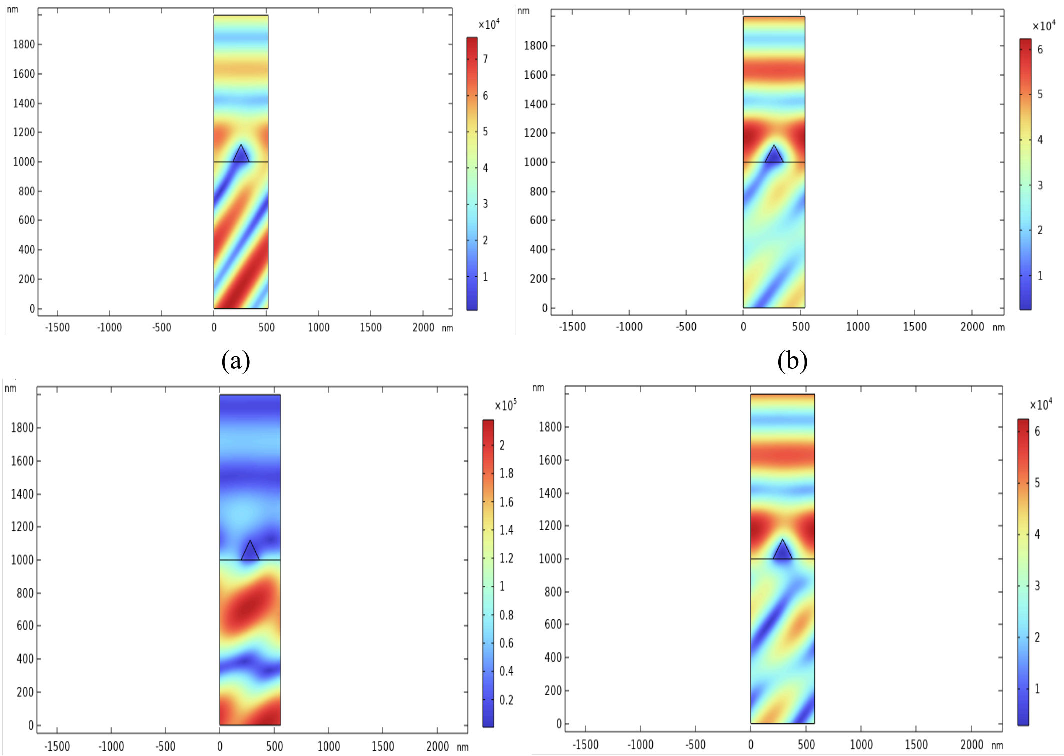

(a) (b)

(c) (d)

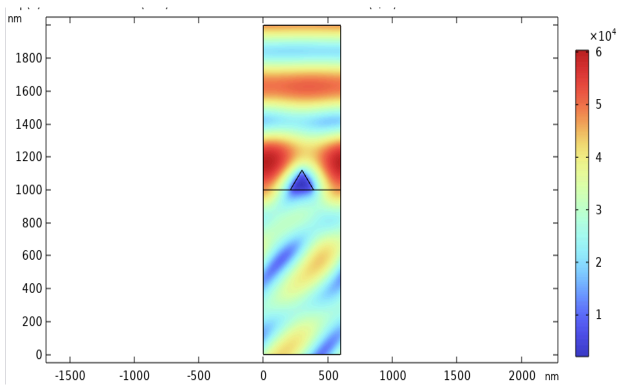

(e)

Fig. 2.4.5 Electric field distribution for the periodicity value of (a) 520 nm (b) 540 nm (c) 560 nm (d) 580 nm and (e) 600 nm.

Like previous cases, variation of periodicity has a deep impact on the values of Figure of Merit. As we increase the periodicity value from 520 nm to 600 nm the max FOM value that we received is 80.28 (RIU) -1 for the value of p=540 nm as shown in table. Variation of FWHM values results in the variation of overall FOM values. The variation of FWHM values with respect to periodicity is portrayed below -

Table 2.4.3: Variation of FOM vs Periodicity

Periodicity (nm)	Figure of Merit (FOM)
520	72.97
540	80.28
560	66.67
580	16.67
600	18.57

As we can see the highest value of FOM is occurring for the periodicity value of 520 nm . However there is a slight reduction of sensitivity value at 520 nm meaning that maximum value of sensitivity and FOM is not occurring for the same periodicity value.

As we can see in Fig. 2.4.6(a) the highest value of FOM occurs at p = 540 nm and as p increases the FOM value decreases and beyond 560 nm it reduces drastically. Similarly for Fig. 2.4.6(b) highest value of sensitivity occurs at 560 nm and as periodicity increases beyond 560 nm it decreases drastically.

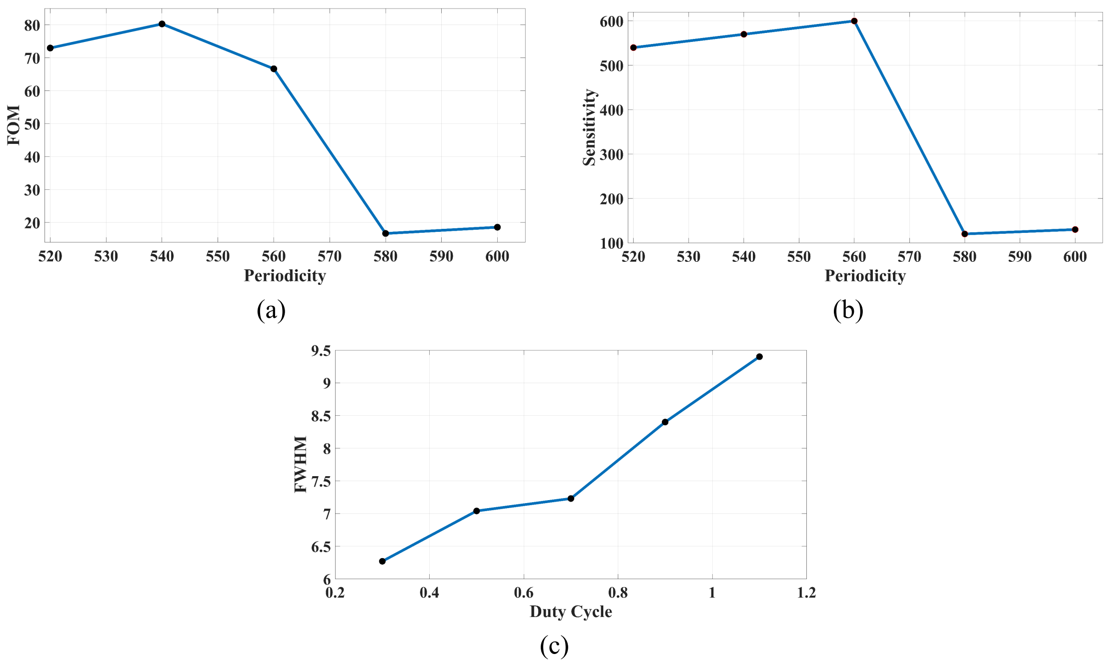

Fig. 2.4.6 (a) Variation of FOM vs Periodicity (b) Variation of Sensitivity vs Periodicity (c) Variation of FWHM with respect to Duty Cycle

With the change of duty cycle from 0.3 to 1.1 we can see that the maximum FWHM value occurs at duty cycle = 1.1. This also affects the overall performance of the SPR sensor.

So overall summary of the performance parameters of the SPR sensor based on triangular grating -

Table 2.4.4: Performance metrics comparison for SPR Sensor based on Triangular Grating

Periodicity (nm)	Sensitivity (nm/RIU)	FOM $(RIU)^{-1}$	Quality Factor (Q)
520	540	72.97	0.729
540	570	80.28	0.803
560	600	66.67	6.67
580	130	16.67	1.67
600	120	18.57	1.86

2.4.3 SPR Sensor Based on Circular Grating

2.4.3.1 Design

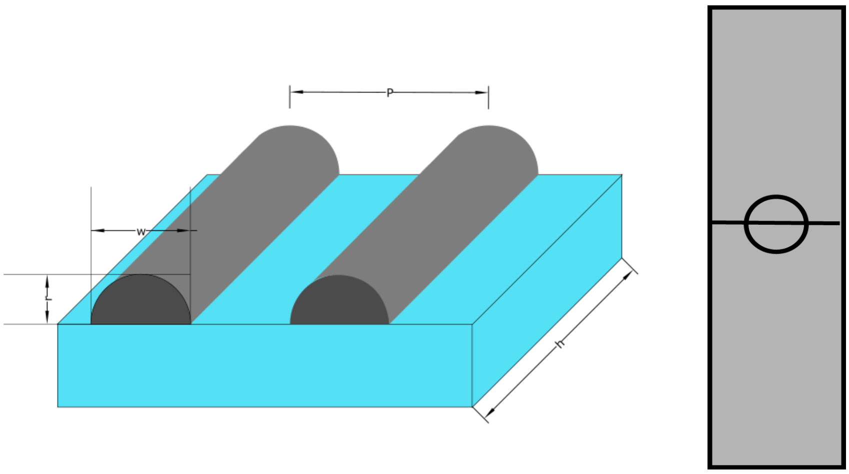

(a) (b)

Fig. 2.4.7 (a) 3D view of circular grating circuit (b) Comsol model for circular grating

Periodic Boundary Condition is applied on both sides of the grating circuit to indicate that the structure is periodically repeated throughout. Gratings are placed periodically on the top of the glass substrate and above that we place a sensing medium. The sensing media can be air or any solution whose change in refractive index will be sensed by the proposed system. The overall system works based on the principle of reversibility. The reflected light intensity peaks at the angle corresponding to light coupling into the waveguide and depends on the effective index of the waveguide mode such that the refractive index is reflected in the spectra by generating an absorption peak at a specific wavelength. The Floquet boundary condition is applied while solving the Maxwell's equation in the system.

P indicates periodicity after which the grating circuits are repeated and the radius of the circular gratings are w/2.

Table 2.4.5: Parameters for Circular Grating

Name	Expression	Value	Description
n_air	1	1	Refractive index of air
n_substrate	1.45	1.45	Refractive index of glass substrate
lambda	500[nm]	0.15μm	Wavelength of incident ray
tm	120[nm]	0.25μm	Height of grating
ts	1[um]	3μm	Height of substrate
h_clad	1000[nm]	3μm	Height of clad layer
a	550[nm]	0.55μm	Slit width
w	p×duty	0.168μm	Grating size
width	w + 2×d	0.56μm	Width of the substrate
p	560 [nm]	0.56μm	Periodicity
n	1	1	Refractive index of the sensing medium
duty	0.3	0.3	Duty cycle
d	$\frac{p-w}{2}$	0.196μm	Gap between grating and boundary

2.4.3.2 Simulation results and analysis

As observed earlier as well for triangular grating, we at first find the parameters of the designed system for the value of periodicity 560 nm.

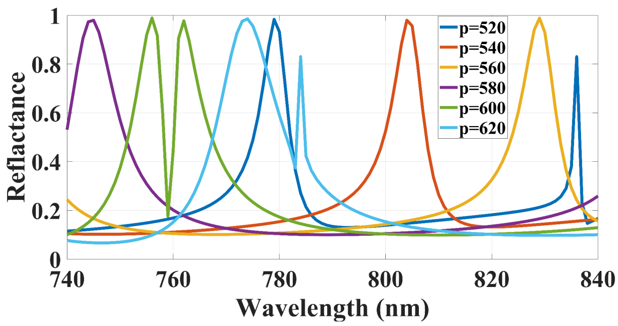

Fig. 2.4.8 Reflection spectra with different periods.

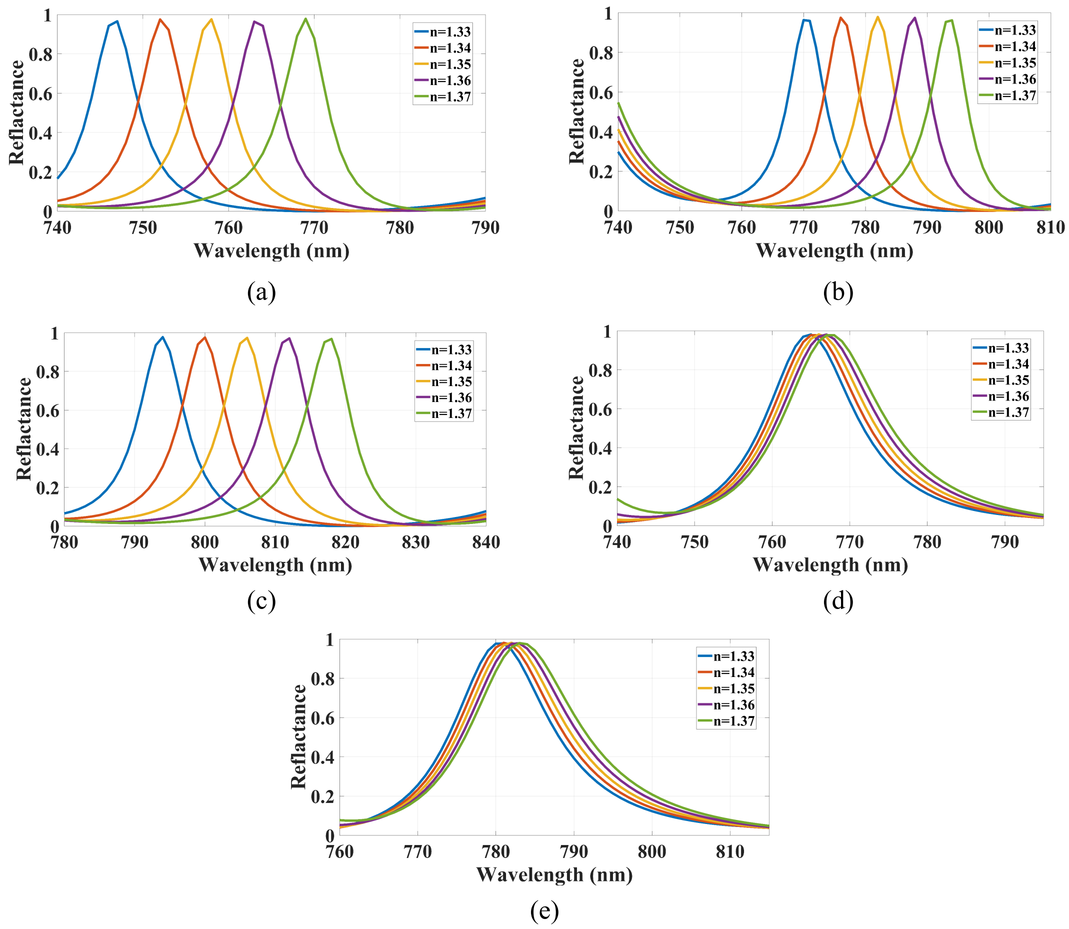

Fig. 2.4.9 Reflection spectra of different values of n for a grating period of (a) 520 nm. (b) 540 nm (c) 560 nm (d) 580 nm and (e) 600 nm

Similar observations like earlier from Fig. 2.4.9(c) we can observe the reflectance profile for the system for a grating period of 560 nm and found out the sensitivity value to be 600 nm/RIU. As we changed the periodicity value from 520 nm to 600 nm the resonant wavelength shifts as portrayed in Fig. 2.4.8.

As we shift the value of periodicity from 520 nm to 600 nm the resonant wavelength range changes from 745 nm to 775 nm for Fig. 2.4.9(a), 750-810 nm for Fig. 2.4.9(b), 780-840 nm for Fig. 2.4.9(c), 740-810 nm for Fig. 2.4.9(d) and 760-830 nm for Fig. 2.4.9(e).

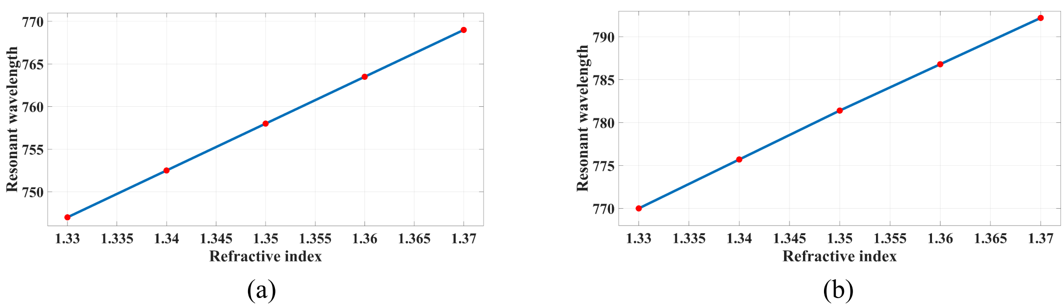

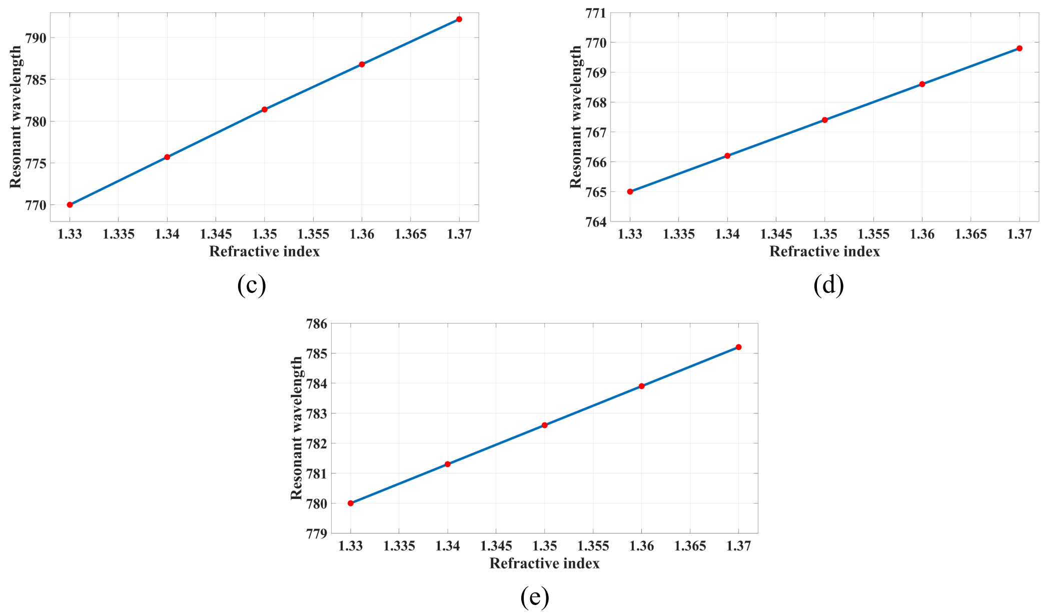

Fig. 2.4.10 Relationship between resonant wavelength and refractive index for grating period of (a) 520 nm (b) 540 nm (c) 560 nm (d) 580 nm and (e) 600 nm

With the change of the periodicity value, the changes in the sensitivity value are documented in the following table -

Table 2.4.6: Variation of Sensitivity with Periodicity values

Periodicity value (nm)	Sensitivity (nm/RIU)
520	550
540	570
560	600
580	110
600	120

Maximum value of sensitivity 600 nm/RIU occurs at p = 560 nm.

As we change the value of the periodicity electric field distribution changes inside the grating circuit. For p = 520 nm in Fig. 2.4.11(a) most of the field energy leaks into the analyte region, maximizing sensitivity. This confirms the system is operating in the desired SPR mode, making it well-suited for refractive index sensing. The field maps depict a standing wave pattern characterized by angled, periodic fringes (alternating red/yellow for high magnitude and blue for low magnitude) in the regions depicted in Fig. 2.4.11(b),(c) and (d) above and below the boundary that contains the small triangular grating element.

This pattern is the result of the interference between the incident wave and the waves reflected and diffracted by the grating structure. show a stable, ordinary wave interference pattern, confirming that the grating system's electromagnetic response is insensitive to this minor variation in the refractive index. That is why for a periodicity value of 560 nm we got the highest value of sensitivity. On the other hand increasing periodicity beyond 560 nm results in significant decrease of sensitivity and FOM values.

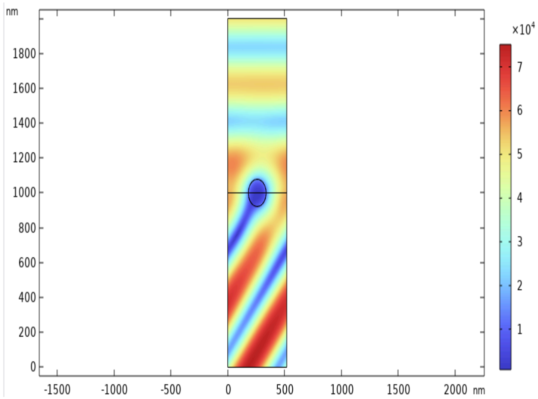

(a)

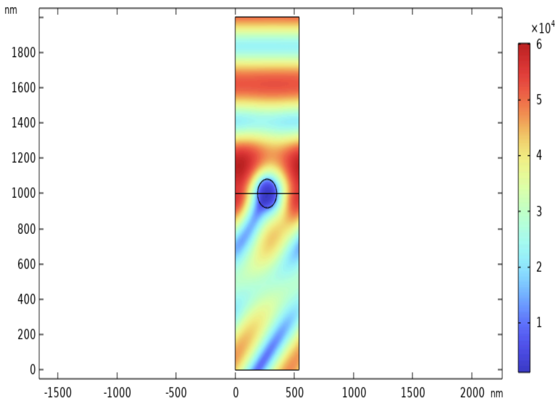

(b)

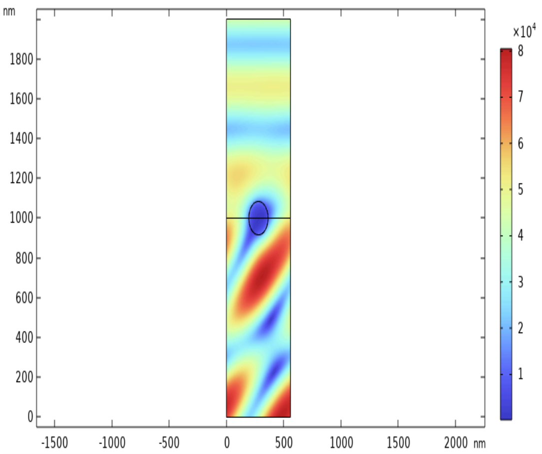

(c)

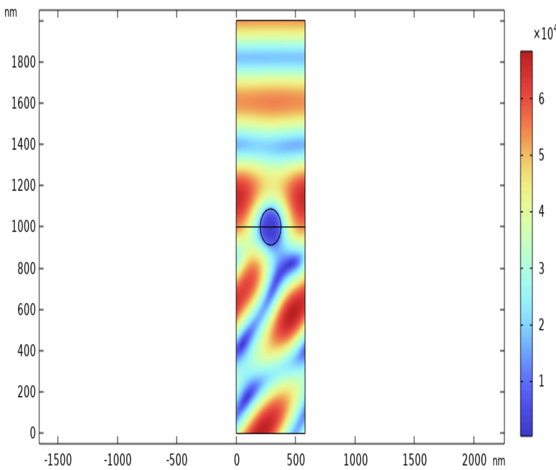

(d)

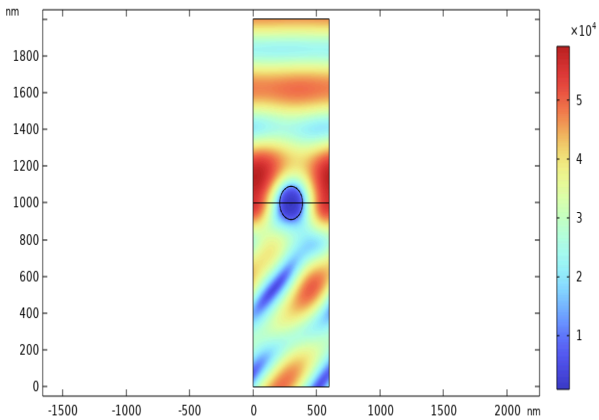

(e)

Fig. 2.4.11 Electric field distribution for the periodicity value of (a) 520 nm (b) 540 nm (c) 560 nm (d) 580 nm and (e) 600 nm.

Like previous cases, variation of periodicity has a deep impact on the values of Figure of Merit. As we increase the periodicity value from 520 nm to 600 nm the max FOM value that we received is 79.71 for the value of p = 520 nm. Variation of FWHM values results in the variation of overall FOM values. The variation of FWHM values with respect to periodicity is portrayed in the following table -

Table 2.4.7: Variation of FOM vs Periodicity

Periodicity (nm)	Figure of Merit (FOM)
520	79.71
540	76.67
560	77.52
580	66.67
600	21.29

As we can see, the highest value of FOM occurs for the periodicity value of 520 nm. However, there is a slight reduction in the sensitivity value at 520 nm, meaning that the maximum value of sensitivity and FOM does not occur for the same periodicity value.

As we can see in Fig. 2.4.12(a), the highest value of FOM occurs at p = 520 nm, and as p increases, the FOM value decreases, and beyond 560 nm it reduces drastically. Similarly, for Fig. 2.4.12(b) highest value of sensitivity occurs at 560 nm and as periodicity increases beyond 560 nm, it decreases drastically.

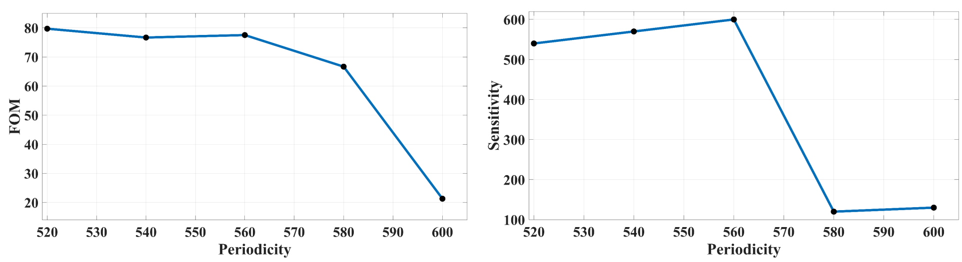

(a) (b)

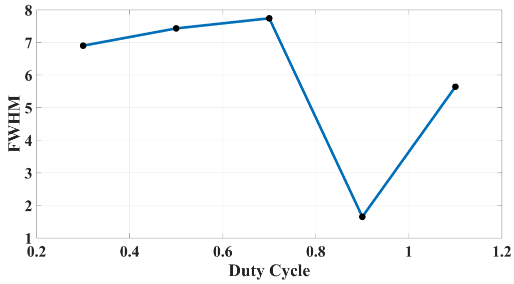

(c)

Fig. 2.4.12 (a) Variation of FOM vs Periodicity (b) Variation of Sensitivity vs Periodicity (c) Variation of FWHM with respect to Duty Cycle

With the change of duty cycle from 0.3 to 1.1 we can see that the maximum FWHM value occurs at duty cycle = 1.1. This also affects the overall performance of the SPR sensor.

Table 2.4.8: Performance metrics comparison for SPR Sensor based on Circular Grating.

Periodicity (nm)	Sensitivity(nm/RIU)	FOM $(RIU)^{-1}$	Quality Factor (Q)
520	540	72.97	0.729
540	570	80.28	0.803
560	600	66.67	6.67
580	130	16.67	1.67
600	120	18.57	1.86

2.4.4 Comparison Between Two Systems and Previous Works

Table 2.4.9: Comparison between circular and triangular grating

Type	**Max Sensitivity (nm/RIU)**	**Max FOM**	**Periodicity (nm)**	**FWHM (nm)**	**Q**
Circular	600	79.71	540	7.10	0.797
Triangular	600	80.28	520	6.25	6.670

Table 2.4.10: Comparison between Previous Literature Works

Reference	Structure	FWHM(nm)	Sensitivity (nm/RIU)	FOM
Gerardo A et al.[29]	Sinusoidal	12	425	35.42
SudhaKumari etal. [30]	Sinusoidal	19	827	45.33
QianshiWanget al. [31]	Sinusoidal	16	961.50	60.09
Tahir Iqbal etal. [32]	Sinusoidal/ Rectangular	10	717	71.70
XuanDouetal. [33]	Sinusoidal	100	1031	10.31
AnujK. Sharmaetal. [34]	Rectangular	24.8	696.66	28.09
ThisWork	Circular	6.25	600	79.91
ThisWork	Triangular	7.10	600	80.28

Chapter 3
Future Work

The sensor designs presented in this work were optimized through parametric sweeps and traditional simulation. A promising direction for future research would be to integrate generative AI models to navigate the design space more comprehensively and discover non-intuitive, high-performance structures. For instance, a framework like Variational MineGAN [10] could be trained on a dataset of high-fidelity simulation results to generate novel, optimized sensor geometries with minimal data requirements, building directly upon the principles established in this thesis.

Chapter 4
Conclusion

This thesis has comprehensively addressed the challenges associated with conventional plasmonic sensors by pioneering innovative designs and exploring alternative materials, leading to significant enhancements in performance, durability, and practical applicability.

The journey began with the design and optimization of a novel Metal-Insulator-Metal (MIM) waveguide-based refractive index sensor. The introduction of a multi-layered composite resonator, integrating nested hexagonal and square cavities, provided a robust platform for strong field confinement. The strategic incorporation of nanorod arrays was a key innovation, systematically investigated to balance the trade-off between sensitivity and resonance linewidth. The optimal configuration with 10 nanorods achieved a peak sensitivity of 1800 nm/RIU and a Figure of Merit (FOM) of 34.0, outperforming many contemporary MIM-based sensor designs documented in the literature. This demonstrates the efficacy of complex, multi-resonant structures in enhancing light-matter interaction for ultrasensitive detection.

A pivotal aspect of this research was the exploration beyond traditional noble metals. The successful implementation of Titanium Nitride (TiN) in an identical sensor geometry yielded a remarkable sensitivity of 1800 nm/RIU. While the FOM was lower than its silver counterpart, this result is profoundly significant. It conclusively validates TiN as a high-performance, CMOS-compatible alternative, offering superior chemical stability, biocompatibility, and thermal resilience, which are critical for real-world biosensing and harsh environment applications.

Concurrently, the project delved into the domain of grating-coupled surface plasmon resonance (GCSPR) sensors. The systematic optimization of both triangular and circular grating geometries revealed the critical dependence of sensitivity and FOM on structural parameters like periodicity and duty cycle. The triangular grating sensor emerged as a standout performer, achieving a sensitivity of 600 nm/RIU coupled with an exceptionally high FOM of 80.28 RIU^{-1}. This performance is highly competitive, surpassing numerous sinusoidal and rectangular gratings reported in prior works, and highlights the potential of simpler, manufacturable geometries for creating compact, label-free sensing platforms.

References

[1] N. L. Kazanskiy, S. N. Khonina, and M. A. Butt, "Plasmonic sensors based on metal-insulator-metal waveguides for refractive index sensing applications: A brief review," Physica E: Low-dimensional Systems and Nanostructures, vol. 114, p. 113798, 2019. doi: 10.1016/j.physe.2019.113798.

[2] A. K. M. Rakib et al., "A numerical analysis of a highly sensitive hexagonal plasmonic refractive index sensor," Optics Communications, vol. 525, p. 129205, 2022. doi: 10.1016/j.optcom.2022.129205.

[3] G. V. Naik, V. M. Shalaev, and A. Boltasseva, "Alternative plasmonic materials: Beyond gold and silver," Advanced Materials, vol. 25, no. 24, pp. 3264–3294, 2013. doi: 10.1002/adma.201205076.

[4] IEEE Journal of Selected Topics in Quantum Electronics, vol. 16, no. 1, pp. 295–306, 2010. doi: 10.1109/jstqe.2009.2034983.

[5] G. Pellegrini et al., "Benchmarking the use of heavily doped Ge for plasmonics and sensing in the mid-infrared," ACS Photonics, vol. 5, no. 12, pp. 4984–4991, 2018. doi: 10.1021/acsphotonics.8b00438.

[6] A. K. M. Rakib, R. Rahad, M. O. Faruque, and R. H. Sagor, "ZrN-based plasmonic sensor: a promising alternative to traditional noble metal-based sensors for CMOS-compatible and tunable optical properties," Optics Express, vol. 31, no. 5, pp. 8618–8633, 2023. doi: 10.1364/OE.494550.

[7] J. Zhang and L. Zhang, "Nanostructures for surface plasmons," in Springer Series in Surface Sciences, vol. 52, 2012.

[8] M. Svedendahl, S. Chen, and M. Käll, "An introduction to plasmonic refractive index sensing," in Plasmonic Sensors and Their Applications, Wiley-VCH, 2021, pp. 1–30.

[9] "Plasmonic wire grating in Comsol," COMSOL Multiphysics® Software, 2023.

[10] Nushin, S. T., Sharar, S. S., & Zahin, F. I. (2025). Variational MineGAN: A data-efficient knowledge transfer architecture for generative AI-assisted design of nanophotonic structures. Optics and Laser Technology, 192, 113685. https://doi.org/10.1016/j.optlastec.2025.113685

[11] X. Wei and S. M. Weiss, "Guided mode biosensor based on grating coupled porous silicon waveguide," Optics Express, vol. 19, no. 12, pp. 11330–11339, 2011.

[12] T. Iqbal and S. Afsheen, "One dimensional plasmonic grating: High sensitive biosensor," Journal of Sensors, vol. 2016, 2016.
[13] M. Hentschel et al., "Transition from isolated to collective modes in plasmonic oligomers," Nano Letters, vol. 10, no. 7, pp. 2721–2726, 2010.
[14] P. O. Patil et al., "Graphene-based nanocomposites for sensitivity enhancement of surface plasmon resonance sensor for biological and chemical sensing: A review," Biosensors and Bioelectronics, vol. 139, p. 111324, 2019.
[15] H. Yuan et al., "Au nanoparticles as label-free competitive reporters for sensitivity enhanced fiber-optic SPR heparin sensor," Biosensors and Bioelectronics, vol. 154, p. 112039, 2020.
[16] K. Lin et al., "Surface plasmon resonance hydrogen sensor based on metallic grating with high sensitivity," Optics Express, vol. 16, no. 23, pp. 18599–18604, 2008.
[17] X. Qi and J. Bi, "Plasmonic sensors relying on nanoparticle arrays created by a template-directed dewetting process," Optics Communications, vol. 453, p. 124328, 2019.
[18] L. Chen, J. Li, J. Liu, and H. Yang, "A Ag–Au bimetallic nanograting surface plasmon resonance sensor based on a prism structure," Optics Communications, vol. 461, p. 125105, 2020.
[19] C. Thirstrup et al., "Diffractive optical coupling element for surface plasmon resonance sensors," Sensors and Actuators B: Chemical, vol. 100, no. 3, pp. 298–308, 2004.
[20] F. C. Chien and S. J. Chen, "A sensitivity comparison of optical biosensors based on four different surface plasmon resonance modes," Biosensors and Bioelectronics, vol. 20, no. 3, pp. 633–642, 2004.
[21] H. Heidarzadeh, "Analysis and simulation of a plasmonic biosensor for hemoglobin concentration detection using noble metal nano-particles resonances," Optics Communications, vol. 459, p. 124940, 2020.
[22] A. L. Gerardo et al., "Recent advances in nanoplasmonic biosensors: applications and lab-on-a-chip integration," Nanophotonics, vol. 6, no. 1, pp. 123–136, 2017.
[23] Y. Sun et al., "Refractive index sensing using the metal layer in DVD-R discs," RSC Advances, vol. 8, no. 48, pp. 27423–27428, 2018.

[24] W. Su, G. Zheng, and X. Li, "Design of a highly sensitive surface plasmon resonance sensor using aluminum-based diffraction grating," Optics Communications, vol. 285, no. 6, pp. 4603–4607, 2012.
[25] S. Nair, C. Escobedo, and R. G. Sabat, "Crossed surface relief gratings as nanoplasmonic biosensors," ACS Sensors, vol. 2, no. 3, pp. 379–385, 2017.
[26] B. W. Liu et al., "A plasmonic sensor array with ultrahigh figures of merit and resonance line widths down to 3 nm," Advanced Materials, vol. 30, no. 13, p. 1706031, 2018.
[27] Q. Wang et al., "Fabrication of silver-silicon gratings for surface plasmon excitation using nanosecond laser interference lithography," Plasmonics, vol. 15, pp. 2071–2080, 2020.
[28] S. Long et al., "Optimization of plasmonic sensors based on sinusoidal and rectangular gratings," Optics Communications, vol. 506, p. 127553, 2022.
[29] G. A. López-Muñoz et al., "A label-free nanostructured plasmonic biosensor based on Blu-ray discs with integrated microfluidics for sensitive biodetection," Biosensors and Bioelectronics, vol. 96, pp. 260–267, 2017.
[30] S. Kumari, S. Mohapatra, and R. S. Moirangthem, "Development of flexible plasmonic plastic sensor using nanograting textured laminating film," Materials Research Express, vol. 4, no. 2, p. 025008, 2017.
[31] T. Iqbal, S. Noureen, S. Afsheen, M. Khan, and M. Ijaz, "Rectangular and sinusoidal Au-grating as plasmonic sensor: A comparative study," Optical Materials, vol. 99, p. 109563, 2020.
[32] X. Dou, P. Y. Chung, P. Jiang, and J. Dai, "Surface plasmon resonance and surface enhanced Raman scattering sensing enabled by digital versatile discs," Applied Physics Letters, vol. 100, no. 4, p. 041116, 2012.
[33] A. K. Sharma and A. K. Pandey, "Self-referenced plasmonic sensor with TiO2 grating on thin Au layer: simulated performance analysis in optical communication band," Journal of the Optical Society of America B, vol. 36, no. 11, pp. F25–F31, 2019.
[34] I. Tathfif, K. S. Rashid, A. A. Yaseer, and R. H. Sagor, "Alternative material titanium nitride based refractive index sensor embedded with defects: An emerging solution in sensing arena," Results in Physics, vol. 43, p. 106073, 2022.

[35] R. Rahad et al., "An alternative plasmonic material-based CMOS-compatible temperature sensor," IEEE Sensors Journal, vol. 21, no. 5, pp. 6100–6107, 2021.
[36] N. L. Kazanskiy, S. N. Khonina, and M. A. Butt, "A numerical investigation of a plasmonic sensor based on a metal–insulator–metal waveguide for simultaneous detection of biological analytes and ambient temperature," Photonics, vol. 8, no. 12, p. 531, 2021.
[37] M. R. Rakhshani, "Tunable and sensitive refractive index sensors by plasmonic absorbers with circular arrays of nanorods and nanotubes for detecting cancerous cells," IEEE Sensors Journal, vol. 18, no. 20, pp. 8454–8461, 2018.
[38] R. A. Mahmud, M. O. Faruque, and R. H. Sagor, "Plasmonic refractive index sensor based on ring-type pentagonal resonator with high sensitivity," Optical and Quantum Electronics, vol. 53, no. 5, p. 256, 2021.
[39] M. Rahmatiyar, M. Afsahi, and M. Danaie, "Design of a refractive index plasmonic sensor based on a ring resonator coupled to a MIM waveguide containing tapered defects," Plasmonics, vol. 15, pp. 2169–2176, 2020.
[40] R. Rahad, A. Ali, M. K. H. Pias, M. A. Islam, and A. Al Fahim, "Plasmonic metal-insulator-metal (MIM) refractive index sensor for glucose level monitoring," Sensors International, vol. 3, p. 100193, 2022.
[41] Rizwanur Rahad, Ahsan Ali, Md. Khaled Hasan Pias, Md. Asadul Islam, Abdullah Al Fahim; Plasmonic Metal‑Insulator‑Metal (MIM) Refractive Index Sensor for Glucose Level Monitoring

Chapter 5
Demonstration of Outcome-Based Education (OBE)

5.1 Introduction

Outcome-Based Education (OBE) is an educational framework designed to align academic learning with the skills and competencies required in the industry. It emphasizes measurable outcomes that students must achieve by the end of a program—such as problem-solving, teamwork, technical proficiency, and effective communication—ensuring graduates are job-ready. In the OBE approach, curricula, teaching strategies, and assessments are all tailored to meet industry standards and expectations, bridging the gap between academic instruction and real-world application.

5.2 Course Outcomes (COs) Addressed

The following table shows the COs addressed in EEE 4700 for Project and Thesis.

COs	CO Statement	POs	Put Tick (√)
			EEE 4800
CO1	Identify a contemporary real life problem related to electrical and electronic engineering by reviewing and analyzing existing research works.	PO2	√
CO2	Determine functional requirements of the problem considering feasibility and efficiency through analysis and synthesis of information.	PO4	√
CO3	Select a suitable solution and determine its method considering professional ethics, codes and standards.	PO8	√
CO4	Adopt modern engineering resources and tools for the solution of the problem.	PO5	√
CO5	Prepare management plan and budgetary implications for the solution of the problem.	PO11	√
CO6	Analyze the impact of the proposed solution on health, safety, culture and society.	PO6	√
CO7	Analyze the impact of the proposed solution on environment and sustainability.	PO7	
CO8	Develop a viable solution considering health, safety,	PO3	

	cultural, societal and environmental aspects.		
CO9	Work effectively as an individual and as a team member for the accomplishment of the solution.	PO9	√
CO10	Prepare various technical reports, design documentation, and deliver effective presentations for demonstration of the solution.	PO10	√
CO11	Recognize the need for continuing education and participation in professional societies and meetings.	PO12	√

5.3 Aspects of Program Outcomes (POs) Addressed

The following table shows the aspects addressed for certain Program Outcomes (POs) addressed in EEE 4700 for Project and Thesis.

	Statement	Different Aspects	Put Tick (√)
PO3	**Design/development of solutions**: Design solutions for complex electrical and electronic engineering problems and design systems, components or processes that meet specified needs with appropriate consideration for public health and safety, cultural, societal, and environmental considerations.	Public health	√
		Safety	√
		Cultural	
		Societal	
		Environmental	√
PO4	**Investigation:** Conduct investigations of complex electrical and electronic engineering problems using research-based knowledge and research methods including design of experiments, analysis and interpretation of data, and synthesis of information to provide valid conclusions.	Design of experiments	√
		Analysis and interpretation of data	√
		Synthesis of information	√
PO6	**The engineer and society:** Apply reasoning informed by contextual knowledge to assess societal, health, safety, legal and cultural issues and the consequent responsibilities relevant to professional engineering practice and solutions to complex electrical and electronic engineering problems.	Societal	√
		Health	√
		Safety	√
		Legal	
		Cultural	

PO7	**Environment and sustainability:** Understand and evaluate the sustainability and impact of professional engineering work in the solution of complex electrical and electronic engineering problems in societal and environmental contexts.	Societal	
		Environmental	√
PO8	**Ethics:** Apply ethical principles embedded with religious values, professional ethics and responsibilities, and norms of electrical and electronic engineering practice.	Religious values	
		Professional ethics and responsibiliti es	
		Norms	
PO10	**Communication:** Communicate effectively on complex engineering activities with the engineering community and with society at large, such as being able to comprehend and write effective reports and design documentation, make effective presentations, and give and receive clear instructions.	Comprehend and write effective reports	√
		Design documentation	√
		Make effective presentations	√
		Give and receive clear instructions	√
PO11	**Project management and finance:** Demonstrate knowledge and understanding of engineering management principles and economic decision-making and apply these to one's own work, as a member and leader in a team, to manage projects and in multidisciplinary environments.	Engineering management principles	√
		Economic decision-making	
		Manage projects	√
		Multidisciplinary environments	√

5.4 Knowledge Profiles (K3 – K8) Addressed

The following table shows the Knowledge Profiles (K3 – K8) addressed in EEE 4700 for Project and Thesis.

K	Knowledge Profile (Attribute)	Put Tick (√)

K3	A systematic, theory-based formulation of engineering fundamentals required in the engineering discipline	√
K4	Engineering specialist knowledge that provides theoretical frameworks and bodies of knowledge for the accepted practice areas in the engineering discipline; much is at the forefront of the discipline	√
K5	Knowledge that supports engineering design in a practice area	√
K6	Knowledge of engineering practice (technology) in the practice areas in the engineering discipline	√
K7	Comprehension of the role of engineering in society and identified issues in engineering practice in the discipline: ethics and the engineer's professional responsibility to public safety; the impacts of engineering activity; economic, social, cultural, environmental and sustainability	√
K8	Engagement with selected knowledge in the research literature of the discipline	√

The following table explains or justifies how the Knowledge Profiles (K3 – K8) have been addressed in EEE 4700/4800 (Project and Thesis).

K	Explanation/Justification
K3	A systematic, theory-based formulation of engineering fundamentals required in the engineering discipline
K4	Engineering specialist knowledge provides theoretical frameworks and bodies of knowledge for the accepted practice areas in the engineering discipline; much is at the forefront of the discipline.
K5	Knowledge that supports engineering design in a practice area
K6	Knowledge of engineering practice (technology) in the practice areas in the engineering discipline
K7	Comprehension of the role of engineering in society and identified issues in engineering practice in the discipline: ethics and the engineer's professional responsibility to public safety; the impacts of engineering activity; economic, social, cultural, environmental, and sustainability
K8	Engagement with selected knowledge in the research literature of the discipline

5.5 Use of Complex Engineering Problems

Our thesis examines designing and optimizing plasmonic refractive index sensors while exploring plasmonic grating circuits through investigating plasmonic materials and alternatives beyond gold and silver. Resolving this complex engineering dilemma demands assimilating progressive principles from nanophotonics, electromagnetics, materials science, and optical engineering. It necessitates employing simulation instruments such as FDTD or COMSOL for modeling and optimization, necessitating analytical and computational dexterity. The study explores innovative plasmonic materials such as aluminum, titanium nitride, and graphene—going beyond conventional gold and silver. This original evaluation of refractive index sensors and grating circuits analyzes cutting-edge materials like aluminum, titanium nitride and graphene to push the boundaries of plasmonic technology

5.6 Socio-Cultural, Environmental, And Ethical Impact

- Nanotechnology needs less amount of space which in turn produces less wastage.
- Less energy requirements results in less power consumption and less carbon footprint.
- Technological Development arises educational opportunities Verification through previous studies by re-simulation

5.7 Attributes of Ranges of Complex Engineering Problem Solving (P1 – P7) Addressed

The following table shows the attributes of ranges of Complex Engineering Problem Solving (P1 – P7) addressed in EEE 4700 for Project and Thesis.

P	**Range of Complex Engineering Problem Solving**	**Put Tick (√)**
Attribute	Complex Engineering Problems have characteristic P1 and some or all of P2 to P7:	
Depth of knowledge required	**P1:** Cannot be resolved without in-depth engineering knowledge at the level of one or more of K3, K4, K5, K6 or K8 which allows a fundamentals-based, first principles analytical approach	√
Range of conflicting requirements	**P2:** Involve wide-ranging or conflicting technical, engineering and other issues	√
Depth of analysis	**P3:** Have no obvious solution and require abstract thinking, originality in analysis to formulate	√

required	suitable models	
Familiarity of issues	**P4:** Involve infrequently encountered issues	√
Extent of applicable codes	**P5:** Are outside problems encompassed by standards and codes of practice for professional engineering	√
Extent of stakeholder involvement and conflicting requirements	**P6:** Involve diverse groups of stakeholders with widely varying needs	√
Interdependence	**P7:** Are high level problems including many component parts or sub-problems	√

The following table explains or justifies how the attributes of ranges of Complex Engineering Problem Solving (P1 – P7) have been addressed in EEE 4700/4800 (Project and Thesis).

P	Explanation/Justification
P1	Cannot be resolved without in-depth engineering knowledge at the level of one or more of K3, K4, K5, K6, or K8 which allows a fundamentals-based, first principles analytical approach
P2	Involve wide-ranging or conflicting technical, engineering, and other issues
P3	Have no obvious solution and require abstract thinking, and originality in analysis to formulate suitable models
P4	Involve infrequently encountered issues
P5	Are outside problems encompassed by standards and codes of practice for professional engineering
P6	Involve diverse groups of stakeholders with widely varying needs
P7	Are high-level problems including many parts or sub-problems

5.8 Attributes of Ranges of Complex Engineering Activities (A1 – A5) Addressed

The following table shows the attributes of ranges of Complex Engineering Activities (A1 – A5) addressed in EEE 4700 for Project and Thesis.

A	Range of Complex Engineering Activities	Put Tick (√)
Attribute	Complex activities means (engineering) activities or projects that have some or all of the following characteristics:	
Range of resources	**A1:** Involve the use of diverse resources (and for this purpose resources include people, money, equipment, materials, information and technologies)	√
Level of interaction	**A2:** Require resolution of significant problems arising from interactions between wide-ranging or conflicting technical, engineering or other issues	√
Innovation	**A3:** Involve creative use of engineering principles and research-based knowledge in novel ways	√
Consequences for society and the environment	**A4:** Have significant consequences in a range of contexts, characterized by difficulty of prediction and mitigation	√
Familiarity	**A5:** Can extend beyond previous experiences by applying principles-based approaches	√

The following table explains or justifies how the attributes of ranges of Complex Engineering Activities (A1 – A5) have been addressed in EEE 4700/4800 (Project and Thesis).

A	Explanation/Justification
A1	Involve the use of diverse resources (and for this purpose resources include people, money, equipment, materials, information, and technologies)
A2	Require resolution of significant problems arising from interactions between wide-ranging or conflicting technical, engineering, or other issues
A3	Involve creative use of engineering principles and research-based knowledge in novel ways
A4	Have significant consequences in a range of contexts, characterized by difficulty of prediction and mitigation
A5	Can extend beyond previous experiences by applying principles-based approaches